

# Comprehensive application of a coupled-channel complex scaling method to the $\bar{K}N-\pi Y$ system

A. Doté<sup>a,b</sup>, T. Inoue<sup>c</sup>, T. Myo<sup>d</sup>

<sup>a</sup>KEK Theory Center, Institute of Particle and Nuclear Studies (IPNS), High Energy Accelerator Research Organization (KEK), 1-1 Oho, Tsukuba, Ibaraki, 305-0801, Japan

<sup>b</sup>J-PARC Branch, KEK Theory Center, IPNS, KEK, 203-1, Shirakata, Tokai, Ibaraki, 319-1106, Japan

<sup>c</sup>Nihon University, College of Bioresource Sciences, Fujisawa 252-0880, Japan

<sup>d</sup>Osaka Institute of Technology, Osaka, Osaka 535-8585, Japan

---

## Abstract

We have applied the coupled-channel complex scaling method (ccCSM) to  $\bar{K}N-\pi Y$  system. One advantage of ccCSM is that resonant states as well as scattering states can be treated in the same framework. For the interactions in the system, we have constructed a meson-baryon potential-matrix by basing on the chiral SU(3) theory and respecting the  $\bar{K}N$  scattering length obtained in the Martin's analysis. For future purpose to apply it more complicated system such as  $\bar{K}NN$ , we adopt a local Gaussian form in the  $r$ -space. We have investigated both the non-relativistic (NR) and the semi-relativistic (SR) kinematics. In the SR case, two types of the potentials are obtained. To test the constructed potentials, we have calculated scattering amplitudes and searched resonances. One resonance pole, corresponding to  $\Lambda(1405)$ , is found in isospin  $I = 0$  system around (1419,  $-20$ ) MeV ((1425,  $-25$ ) or (1419,  $-13$ ) MeV) on complex-energy plane with the NR (SR) kinematics. Mean distance between meson and baryon in the resonant state is  $1.3 - i0.3$  fm ( $1.2 - i0.5$  fm) for NR (SR), in which the states are treated as Gamow states. In addition, we have observed a signature of another pole in lower-energy region involving large decay width, although they are unstable against the change of scaling angle  $\theta$ . This may correspond to the lower pole of the double-pole of  $\Lambda(1405)$  discussed in literature to date.

*Keywords:* Complex scaling method,  $\bar{K}N-\pi Y$  system,  $\Lambda(1405)$ , Scattering amplitude, Chiral SU(3) theory

---

## 1. Introduction

$\bar{K}$ -nuclear system has been a hot topic in nuclear and hadron physics for a long time. Due to strongly attractive  $\bar{K}N$  interaction in isospin  $I = 0$  channel, finite nuclear systems with anti-kaons are expected to have exotic properties such as deeply bound and quasi-stable states with high density [1, 2]. Such kaonic nuclei have been investigated with various many-body treatments [2, 3, 4]. In particular, to clarify the property of kaonic nuclei, great efforts have been devoted to investigate  $K^-pp$ <sup>1</sup>, a prototype of kaonic nuclei, in both of theoretical and experimental studies. From the theoretical studies, it has been claimed that  $K^-pp$  will not be so deeply bound and its decay width will be large (total binding energy  $< 100$  MeV and decay width  $> 50$  MeV) [1, 5, 6, 7, 8, 9], although there are quantitative discrepancies between calculations [10]. On the other hand, experimental results indicate deeper binding of  $K^-pp$  than theoretical predictions if the observed state is the bound  $K^-pp$  [11, 12], although there are some objections to the experimental result [13]. Thus, the consensus for  $K^-pp$  has not been achieved yet.

For study of kaonic nuclei,  $\bar{K}N$  (involving  $\pi Y$ ) interaction is a basic input, and a  $\Lambda(1405)$  resonance is an essential building block because it can be reasonably interpreted as a quasi-bound  $I = 0$  state of  $\bar{K}N$  with  $s$ -wave, rather than a three-quark state [14]. One approach to  $\bar{K}N$  system is a study based on the chiral SU(3) coupled-channel dynamics [15]. This approach (called the chiral unitary model by Oset and Ramos [16]) has been succeeded in studies of  $s$ -wave meson-baryon systems including  $S = -1$  sector [17]. The double pole nature of  $\Lambda(1405)$  pointed out within this model, is interesting [18, 19]. According to further studies along this model, some experimental data seem to support the double-pole nature [20]. Ref. [21], however, shows that the current low-energy observables are not so precise to distinguish whether  $\Lambda(1405)$  is single pole or double pole. Thus, the  $\Lambda(1405)$ -pole problem has not been solved yet. Recently, accurate data at the  $\bar{K}N$  threshold are given by a precise measurement of  $1s$  level shift of kaonic hydrogen atom [22], in addition to experimental data on  $\bar{K}N$  subthreshold region [23] and old data on  $K^-p$  branching ratio [24]. Due to such precise data, the physical quantities near the  $\bar{K}N$  threshold are strictly constrained

---

<sup>1</sup>Actually, this system is a  $\bar{K}NN$ - $\pi YN$  coupled system with quantum numbers  $J^\pi = 0^-$ ,  $(T, T_z) = (1/2, 1/2)$ . It is expressed symbolically as  $K^-pp$ .

and those uncertainties below the  $\bar{K}N$  threshold are also expected to be decreased [25].

In such a current situation, we start a study of kaonic nuclei with a coupled-channel complex scaling method (ccCSM), keeping in mind the following three points: 1. Simple and adequate treatment of resonant states in many-body system, 2. Explicit inclusion of all channels in a coupled-channel problem, and 3. Accessible to structure of kaonic nuclei. Looking back past studies on  $K^-pp$ , in variational studies [1, 7] it is treated as a bound state in  $\bar{K}NN$  channel as a consequence of the elimination of  $\pi Y$  channels. In Faddeev-AGS studies [5, 6] certainly a coupled-channel calculation is fully performed and resonance poles are searched. However, there a separable form is assumed to the  $\bar{K}N-\pi Y$  potential which is a key ingredient in the  $\bar{K}$ -nuclear study, and a wave function is not obtained explicitly in this approach though it is important to investigate the nature of kaonic nuclei. Thus, each approach involves advantages and disadvantages. Since the ccCSM is expected to overcome above disadvantages, we employ this method to study the  $\bar{K}$ -nuclear system.

The complex scaling method (CSM) has been applied to various nuclear physics, and it has been greatly succeeded in particular in the study of resonant states of unstable nuclei [26]. The CSM is a practical tool for the study of nuclear many-body systems. Indeed, a resonance nature in unstable  ${}^8\text{He}$  is revealed with the CSM in Ref. [27] where a five-body system of  ${}^4\text{He} + n + n + n + n$  is solved. The CSM is suitable for resonant states, because we can handle them in the same way as bound states. Though a resonant wave function is originally divergent at infinite distance, in the CSM it is transformed to a square-integrable function by a complex rotation for the coordinate and then it can be represented with *e.g.* a Gaussian base which is familiar for ones study bound states. In addition, by an advanced used of complex-rotated wave functions, the scattering amplitude can also be calculated with the Gaussian base [28]. Thus, all of bound, resonant and scattering states can be handled in a single framework of the CSM with Gaussian base.

Since it is our first attempt applying the ccCSM to  $\bar{K}$ -nuclear systems, in this article we investigate the *s*-wave two-body system of  $\bar{K}N-\pi Y$  coupled channels. We examine semi-relativistic kinematics as well as non-relativistic one to be careful of a pion which is a light-mass particle. First, we will check how the ccCSM works in the present system. Then, we will construct a meson-baryon potential for the  $\bar{K}N-\pi Y$  coupled system, based on a chiral

SU(3) theory. We adopt a Gaussian-form potential in the coordinate space, because of convenience for our further study of  $\bar{K}$ -nuclear system with Gaussian base. Our potential is constrained by the  $\bar{K}N$  scattering lengths for both isospin states obtained by the Martin's analysis of old  $\bar{K}N$  scattering data [29]. Using the constructed potential, we will investigate the behavior of the scattering amplitude. In the  $I = 0$  sector, the pole on the complex-energy plane also will be investigated in detail because there should be a resonance corresponding to the  $\Lambda(1405)$ .

The contents of the article are as follows: In the section 2, we will explain a meson-baryon potential used in our study and the formalism of ccCSM for the study of scattering state as well as resonant state in detail. In the section 3, the obtained results will be given. The scattering amplitudes will be shown for both isospin states. For the  $I = 0$  channel, the structure of a resonant state will be investigated. In the last section, we will mention our summary and future plans including some discussions.

## 2. Formalism

### 2.1. Kinematics and interaction

We are considering a  $\bar{K}N$ - $\pi Y$  coupled system in  $s$ -wave, where  $Y$  indicates a hyperon which is  $\Sigma$  ( $\Lambda$  and  $\Sigma$ ) for  $I = 0$  ( $I = 1$ ) case. We investigate such a two-body system in semi-relativistic kinematics as well as non-relativistic one, because a pion joins in our calculation and its mass is very small. The Hamiltonian for non-relativistic kinematics is

$$\hat{H} = \sum_{\alpha} \left( M_{\alpha} + m_{\alpha} + \frac{\hat{\mathbf{p}}_{\alpha}^2}{2\mu_{\alpha}} \right) |\alpha\rangle\langle\alpha| + \hat{V}_{MB}^{NR}, \quad (1)$$

and that for semi-relativistic kinematics is

$$\hat{H} = \sum_{\alpha} \left( \sqrt{M_{\alpha}^2 + \hat{\mathbf{p}}_{\alpha}^2} + \sqrt{m_{\alpha}^2 + \hat{\mathbf{p}}_{\alpha}^2} \right) |\alpha\rangle\langle\alpha| + \hat{V}_{MB}^{SR}. \quad (2)$$

Here  $M_{\alpha}$ ,  $m_{\alpha}$  and  $\mu_{\alpha}$  are baryon, meson and a reduced mass in the channel  $\alpha$ , respectively.  $\hat{\mathbf{p}}_{\alpha}$  is the relative momentum between a meson and a baryon in the channel  $\alpha$ .

The last term  $\hat{V}_{MB}^{NR}$  ( $\hat{V}_{MB}^{SR}$ ) represents a meson-baryon potential for non-relativistic (semi-relativistic) kinematics. In Ref. [15], Kaiser, Siegel and Weise (KSW) proposed a pseudo-potential for  $s$ -wave meson-baryon system

with  $S = -1$  derived from an effective chiral SU(3) Lagrangian, and used it in the Lippmann-Schwinger equation to obtain  $\Lambda(1405)$ . The pseudo-potential consists of all terms up to order  $q^2$  allowed by chiral symmetry. They introduced two kinds of cut-off; one is projection to a Yukawa form local potential in the  $r$ -space and another is casting to a separable potential in the  $p$ -space. In this paper, we follow KSW work and adopt the leading Weinberg-Tomozawa term of the pseudo-potential:

$$\hat{V}_{MB}^{SR} = \sum_{\alpha,\beta} -\frac{C_{\alpha\beta}^I}{8f_\pi^2}(\omega_\alpha + \omega_\beta) \sqrt{\frac{M_\alpha M_\beta}{s \tilde{\omega}_\alpha \tilde{\omega}_\beta}} g_{\alpha\beta}^I(r) |\alpha\rangle\langle\beta|, \quad (3)$$

$$g_{\alpha\beta}^I(r) = (\sqrt{\pi} d_{\alpha\beta}^I)^{-3} \exp[-(r/d_{\alpha\beta}^I)^2]. \quad (4)$$

For a cut-off form factor, we introduce the local Gaussian function  $g_{\alpha\beta}^I(r)$  in  $r$ -space with a range parameter  $d_{\alpha\beta}^I$ . Hereafter, we denote this potential as “KSW-type potential”. Note that this potential is energy dependent because meson energy  $\omega_\alpha$ , baryon energy  $E_\alpha$  and the reduced energy  $\tilde{\omega}_\alpha = \omega_\alpha E_\alpha / (\omega_\alpha + E_\alpha)$  are given by function of CM energy  $\sqrt{s}$  as follows:

$$E_\alpha = \frac{(\sqrt{s})^2 - m_\alpha^2 + M_\alpha^2}{2\sqrt{s}} \quad \text{and} \quad \omega_\alpha = \frac{(\sqrt{s})^2 + m_\alpha^2 - M_\alpha^2}{2\sqrt{s}}. \quad (5)$$

Note also that structure of this potential is determined by the coefficients  $\{C_{\alpha\beta}^I\}$  which are computed by Clebsch-Gordan coefficients of SU(3) and given as

$$C^{(I=0)} = \begin{pmatrix} \bar{K}N & \pi\Sigma \\ 3 & -\sqrt{3/2} \\ & 4 \end{pmatrix}, \quad C^{(I=1)} = \begin{pmatrix} \bar{K}N & \pi\Sigma & \pi\Lambda \\ 1 & -1 & -\sqrt{3/2} \\ & 2 & 0 \\ & & 0 \end{pmatrix}. \quad (6)$$

Strength of this potential depends on the pion decay constant  $f_\pi$ . It is noted that the range parameter  $d_{\alpha\beta}^I$  can be a different value in each channel set  $(\alpha, \beta)$ . For the range parameter of the transition potential, we assume that  $d_{\alpha\beta}^I = (d_{\alpha\alpha}^I + d_{\beta\beta}^I)/2$  to reduce the number of parameters.

Since the flux factor  $\sqrt{\frac{M_\alpha M_\beta}{s \tilde{\omega}_\alpha \tilde{\omega}_\beta}}$  in Eq. (3) is based on the relativistic kinematics, the KSW-type potential had better be used in the semi-relativistic framework in our calculation. When we adopt the non-relativistic kinematics, we make non-relativistic reduction to the flux factor in two prescriptions,

denoted as “NRv1” and “NRv2”. In the first prescription, comparing the expression of the differential cross section in both kinematics, we replace the reduced energy in Eq. (3) with the reduced mass;

$$\text{NRv1 : } \hat{V}_{MB}^{NRv1} = \sum_{\alpha,\beta} -\frac{C_{\alpha\beta}^I}{8f_\pi^2}(\omega_\alpha + \omega_\beta) \sqrt{\frac{M_\alpha M_\beta}{s \mu_\alpha \mu_\beta}} g_{\alpha\beta}^I(r) |\alpha\rangle\langle\beta|. \quad (7)$$

In the second prescription, by considering the small momentum limit, we replace the meson and baryon energies with the meson and baryon masses, respectively;

$$\text{NRv2 : } \hat{V}_{MB}^{NRv2} = \sum_{\alpha,\beta} -\frac{C_{\alpha\beta}^I}{8f_\pi^2}(\omega_\alpha + \omega_\beta) \sqrt{\frac{1}{m_\alpha m_\beta}} g_{\alpha\beta}^I(r) |\alpha\rangle\langle\beta|. \quad (8)$$

In both non-relativistic approximations, we keep remaining the meson-energy part  $(\omega_\alpha + \omega_\beta)$  as original, because this energy dependence is attributed to the chiral dynamics which we respect in our study. Of course, energies such as  $\sqrt{s}$  and  $\omega_\alpha$  themselves, are calculated by the non-relativistic formula.

We remark the normalization of the pseudo-potentials used in this article. All pseudo-potentials, given in Eqs. (3, 7, 8), are normalized so that we obtain  $3\mu/(8\pi f_\pi^2)$  for the scattering length of isoscalar  $\bar{K}N$  in the Born approximation and the formula of scattering amplitude (27) which will be explained in the next section. Here,  $\mu$  is the reduced mass of anti-kaon and a nucleon.

## 2.2. Coupled-channel complex scaling method

As mentioned in the introduction, the  $s$ -wave  $\bar{K}N$ - $\pi\Sigma$  system has a resonant state in  $I = 0$  channel which corresponds to the  $\Lambda(1405)$ . Such a resonant state of a meson-baryon system can be investigated with the complex scaling method (CSM), in the same way as resonant states of unstable nuclei. Here, we give a brief explanation of the coupled-channel complex scaling method (ccCSM). Details of the CSM and its successful application to unstable nuclear physics are summarized in Ref. [26]

In the CSM, a relative coordinate  $\mathbf{r}$  and a conjugate wave number  $\mathbf{k}$  in Hamiltonian  $\hat{H}$  and a wave function  $|\Phi\rangle$  are complex-scaled as

$$U(\theta) : \mathbf{r} \rightarrow \mathbf{r}e^{i\theta}, \mathbf{k} \rightarrow \mathbf{k}e^{-i\theta}. \quad (9)$$

Then, transformed Hamiltonian and wave function are defined as  $\hat{H}_\theta \equiv U(\theta)\hat{H}U^{-1}(\theta)$  and  $|\Phi_\theta\rangle \equiv U(\theta)|\Phi\rangle$ , respectively. We expand the wave function  $\Phi(\mathbf{r})$  in partial waves as  $\Phi(\mathbf{r}) = \sum_{lm} \phi_l(r)/r Y_{lm}(\Omega)$  as usual. In our definition, all radial wave functions are transformed by the complex scaling operator as

$$\phi_l^\theta(r) \equiv U(\theta)\phi_l(r) = e^{i\theta/2}\phi_l(re^{i\theta}), \quad (10)$$

taking into account the Jacobian in integration to calculate expectation value of operators. An expectation value of operator  $\hat{O}$  is calculated with bi-orthogonal set  $\{\tilde{\Phi}_\theta, \Phi_\theta\}$ :

$$\langle \hat{O} \rangle_\theta \equiv \langle \tilde{\Phi}_\theta | \hat{O} | \Phi_\theta \rangle, \quad (11)$$

where  $\tilde{\Phi}_\theta(r) = \Phi_\theta^*(r)$  in terms of radial part of wave function for bound and resonant states. The complex scaled wave function is generally normalized as  $\langle \tilde{\Phi}_\theta | \Phi_\theta \rangle = 1$ . With the definition of the bi-orthogonal state, the radial part of the complex scaled wave function is normalized as

$$\sum_l \int_0^\infty dr \{ \phi_l^\theta(r) \}^2 = 1 \quad (12)$$

for bound and resonant states [30].

It is known that energies of bound and resonant states are independent of the scaling angle  $\theta$  while those of continuum states vary with  $\theta$  as  $\frac{k^2}{2m}e^{-2i\theta}$  in case of non-relativistic kinematics (*ABC theorem* [26]). In addition, it is easily understood that a resonant wave function is transformed from a divergent function to a damped function by the complex scaling  $U(\theta)$  with adequate values of  $\theta$ . In other words, the boundary condition for resonant states is modified to the same one for bound states. Therefore, we can obtain resonant states as follows: For various  $\theta$ 's, complex eigenvalues are calculated by diagonalizing the complex-scaled Hamiltonian  $\hat{H}_\theta$  with Gaussian base as done in usual studies of bound states. Among obtained eigenstates, the states with the eigenvalues independent of  $\theta$  are recognized as resonant states. Since the continuum states appear along a line  $\tan^{-1}(\text{Im } E / \text{Re } E) = -2\theta$  on the complex-energy plane, resonant states can be separated from the continuum states when we set the scaling angle  $\theta$  appropriately. Similarly, resonant states can be found also in case of semi-relativistic kinematics, although complex eigenvalues of continuum states have different  $\theta$  dependence from non-relativistic case.

In the present study, the CSM is applied to a coupled-channel problem, because the  $I = 0$  wave function contains the  $\bar{K}N$  and  $\pi\Sigma$  components. The spatial parts of these wave functions with  $s$ -wave,  $\phi_{\bar{K}N}(r)$  and  $\phi_{\pi\Sigma}(r)$ , are expanded with Gaussian base  $G_n^\alpha(r)$ :

$$|\Phi_{\bar{K}N-\pi\Sigma}^{I=0,l=0}\rangle = \frac{1}{r}\phi_{\bar{K}N}^{l=0}(r)Y_{00}(\Omega)|\bar{K}N\rangle + \frac{1}{r}\phi_{\pi\Sigma}^{l=0}(r)Y_{00}(\Omega)|\pi\Sigma\rangle \quad (13)$$

$$\phi_\alpha^{l=0}(r) = \sum_j C_j^\alpha G_j(r) = \sum_j C_j^\alpha N_{l=0}(b_j) r \exp[-r^2/2b_j^2], \quad (14)$$

where coefficients  $\{C_n^\alpha\}$  are complex parameters to be determined. As explained above, by diagonalizing the  $\hat{H}_\theta$  with the basis  $\{G_n^\alpha(r)|\alpha\rangle\}$  and investigating the  $\theta$  dependence of eigenvalues, we can find resonant states. As explained in Eq. (12), the radial part of the  $I = 0$  wave function (Eq. (13)) is normalized as

$$\int_0^\infty dr \left[ \left\{ \phi_{\bar{K}N,\theta}^{l=0}(r) \right\}^2 + \left\{ \phi_{\pi\Sigma,\theta}^{l=0}(r) \right\}^2 \right] = 1, \quad (15)$$

when it is complex-scaled.

Note that the self-consistency for the complex energy is needed to be considered, since the meson-baryon potentials (Eqs. (3), (7) and (8)) have an energy dependence attributed to chiral dynamics. The eigen-energy  $E_{calc}$  of Hamiltonian calculated with the ccCSM should coincide with the energy  $E_{int}$  input of the meson-baryon potential  $\hat{V}_{MB}(\sqrt{s} = E_{int})$ . Here  $E_{calc}$  and  $E_{int}$  are complex values because they are the energies of resonant states,  $E_R - i\Gamma/2$ . ( $E_R$  and  $\Gamma$  are energy and decay width, respectively.) At the  $n$ -th iteration, we set a value of  $E_{int}^{(n)}$  as an input for  $\hat{V}_{MB}$  and then obtain an eigen-energy  $E_{calc}^{(n)}$  of resonant state with ccCSM. We use  $E_{calc}^{(n)}$  as an input  $E_{int}^{(n+1)}$  for the next turn. Such iterations are repeated until the self-consistent condition is satisfied;  $E_{calc}^{(n)} = E_{int}^{(n)}$ . In case of the present system, the self-consistency is achieved in five-times iterations [31] ( $n \leq 5$ ).

### 2.3. Scattering amplitude calculated with ccCSM — “CS-WF” method

We are interested in the scattering state as well as the resonant state which can be investigated with the usual CSM as explained in the previous section. In this article, we solve a scattering problem also with a square-integrable base such as Gaussian base with the help of the CSM, following a method called “CS-WF” which was developed by Kruppa, Suzuki and Kato

[28]. Here, the detailed formalism of CS-WF is shown for a multi-channel case such as the  $\bar{K}N\text{-}\pi Y$  system.

We assume a system involving  $n$  channels in which the channel  $c_0$  is the incident channel with the energy  $E$ . In a non-relativistic case, the radial Schrödinger equation for such a multi-channel system is

$$(E - H_c^l)\Phi_{l,c}^{(c_0)}(r) = \sum_{c'=1}^n V_{cc'}\Phi_{l,c'}^{(c_0)}(r), \quad (16)$$

$$H_c^l = -\frac{\hbar^2}{2\mu_c} \frac{d^2}{dr^2} + \frac{\hbar^2}{2\mu_c} \frac{l(l+1)}{r^2} + V_{D,c}(r) + M_{T,c}, \quad (17)$$

where  $\mu_c$  and  $M_{T,c}$  are the reduced mass and the total mass in the channel  $c$ , respectively.  $V_{D,c}(r)$  is a direct potential for the channel  $c$  and  $V_{cc'}$  is a transition potential between channels  $c$  and  $c'$ . We assign closed (open) channels for the incident energy  $E$  to channel numbers  $c = 1, \dots, n_B$  ( $c = n_B + 1, \dots, n$ ). The wave function of the channel  $c$  can be written as

$$\Phi_{l,c}^{(c_0)}(r) = \begin{cases} \psi_{l,c}^{(c_0),B}(r) & (c = 1, \dots, n_B) \\ \hat{j}_l(k_{c_0}r) \delta_{c,c_0} + \psi_{l,c}^{(c_0),sc}(r) & (c = n_B + 1, \dots, n) \end{cases}, \quad (18)$$

where  $\hat{j}_l(kr)$  is the Riccati-Bessel function. The incident wave number  $k_{c_0}$  satisfies  $\frac{\hbar^2}{2\mu_{c_0}}k_{c_0}^2 + M_{T,c_0} = E$ .

Inserting this equation into Eq. (16) and applying the complex scaling, then we obtain the coupled equations as follows:

$$\begin{aligned} & (E - H_c^{l,\theta}) \begin{Bmatrix} \psi_{l,c}^{(c_0),B,\theta}(r) \\ \psi_{l,c}^{(c_0),sc,\theta}(r) \end{Bmatrix} \\ & - \sum_{c'=1}^{n_B} V_{cc'}(re^{i\theta})\psi_{l,c'}^{(c_0),B,\theta}(r) - \sum_{c'=n_B+1}^n V_{cc'}(re^{i\theta})\psi_{l,c'}^{(c_0),sc,\theta}(r) \\ & = e^{i\theta/2}V_{cc_0}(re^{i\theta})\hat{j}_l(kre^{i\theta}) \begin{Bmatrix} (c = 1, \dots, n_B) \\ (c = n_B + 1, \dots, n) \end{Bmatrix}, \end{aligned} \quad (19)$$

where  $\psi_{l,c}^{(c_0),B,\theta}(r)$  ( $\psi_{l,c}^{(c_0),sc,\theta}(r)$ ) means the  $\psi_{l,c}^{(c_0),B}(r)$  ( $\psi_{l,c}^{(c_0),sc}(r)$ ) complex-scaled as following Eq. (10). The complex-scaled Hamiltonian for the channel  $c$  is

$$H_c^{l,\theta} = -e^{-2i\theta} \frac{\hbar^2}{2\mu_c} \frac{d^2}{dr^2} + e^{-2i\theta} \frac{\hbar^2}{2\mu_c} \frac{l(l+1)}{r^2} + V_{D,c}(re^{i\theta}) + M_{T,c}. \quad (20)$$

The wave functions for the closed channels,  $\{\psi_{l,c}^{(c_0),B}(r)\}$ , are square-integrable since the threshold energy of these channels is above the incident energy  $E$ . The complex-scaled ones are also square-integrable. As for the open channels whose threshold energies are below the  $E$ , the scattered part of wave functions,  $\{\psi_{l,c}^{(c_0),sc}(r)\}$ , are not square-integrable, since they behave in the asymptotic region as

$$\psi_{l,c}^{(c_0),sc}(r) \rightarrow k_c f_{l,cc_0}(k_c) \hat{h}_l^{(+)}(k_c r) \propto \exp\{i(k_c r - l\pi/2)\} \quad \text{at } r \rightarrow \infty, \quad (21)$$

where  $\hat{h}_l^{\pm}(kr)$  is the Riccati-Hankel function. But, they are transformed to be square-integrable functions due to the complex scaling. The asymptotic behavior of the complex-scaled scattered part of wave function is

$$\psi_{l,c}^{(c_0),sc,\theta}(r) \propto i^{-l} \exp\{ik_c r \cos \theta - k_c r \sin \theta\} \quad \text{at } r \rightarrow \infty. \quad (22)$$

It is easy to understand that the  $\psi_{l,c}^{(c_0),sc,\theta}$  becomes a square-integrable function for  $0 < \theta < \pi$ . Thus, since both the complex-scaled wave functions  $\{\psi_{l,c}^{(c_0),B,\theta}(r)\}$  and  $\{\psi_{l,c}^{(c_0),sc,\theta}(r)\}$  are square-integrable, they can be expanded with Gaussian base  $\{G_i(r)\}$  as

$$\begin{Bmatrix} \psi_{l,c}^{(c_0),B,\theta}(r) \\ \psi_{l,c}^{(c_0),sc,\theta}(r) \end{Bmatrix} \equiv \psi_{l,c}^{(c_0),\theta}(r) = \sum_{j=1}^N t_{c,j}^{(c_0)}(\theta) G_j(r). \quad (23)$$

In the present study, we use a common set of normalized Gaussians for all channels:

$$G_i(r) = N_i(b_i) r^{l+1} \exp\left[-\frac{r^2}{2b_i^2}\right], \quad N_i(b_i) = b_i^{-(2l+3)/2} \left\{ \frac{2^{l+2}}{(2l+1)!!\sqrt{\pi}} \right\}^{1/2}. \quad (24)$$

Inserting the Eq. (23) into the coupled equations (19), linear equations for the unknown variables  $\{t_{c,i}^{(c_0)}(\theta)\}$  are obtained:

$$\sum_j \left[ \left( E O_{ij} - H_{c,ij}^{l,\theta} \right) t_{c,j}^{(c_0)}(\theta) - \sum_{c'=1}^n V_{cc',ij}^\theta t_{c',j}^{(c_0)}(\theta) \right] = b_{cc_0,i}^\theta, \quad (25)$$

where each matrix element indicates  $O_{ij} = \langle G_i | G_j \rangle$ ,  $H_{c,ij}^{l,\theta} = \langle G_i | H_c^{l,\theta} | G_j \rangle$ ,  $V_{cc',ij}^\theta = \langle G_i | V_{cc'}(r e^{i\theta}) | G_j \rangle$  and

$$b_{cc_0,i}^\theta = e^{i\theta/2} \int_0^\infty dr G_i(r) V_{cc_0}(r e^{i\theta}) \hat{j}_l(kr e^{i\theta}). \quad (26)$$

We explain how to calculate scattering amplitudes in the remaining part of this section. With the scattering wave functions  $\{\Phi_{l,c}^{(c_0)}(r)\}$ , the scattering amplitude between the initial channel  $c_0$  and the final channel  $c$  is expressed as

$$f_{l,cc_0}(k_c) = -\frac{2\mu_c}{\hbar^2 k_c k_{c_0}} \sum_{c'=1}^n \int_0^\infty dr \hat{j}_l(k_c r) V_{cc'}(r) \Phi_{l,c'}^{(c_0)}(r). \quad (27)$$

It is obtained with the help of Green function, as a detailed explanation is given in Appendix A. By inserting Eq. (18) into the  $\Phi_{l,c'}^{(c_0)}(r)$  of the above equation, the full scattering amplitude is decomposed to the Born term  $f_{l,cc_0}^{Born}(k_c)$  attributed to the incoming wave  $\hat{j}_l(k_{c_0} r)$  and the other part  $f_{l,cc_0}^{sc}(k_c)$  attributed to the scattered wave  $\psi_{l,c}^{(c_0)}(r)$ . The Born term can be obtained by the numerical integration. In the calculation of  $f_{l,cc_0}^{sc}(k_c)$ , the integration path can be modified from  $r$ -axis to  $re^{i\theta}$ -line due to the Cauchy's theorem. Therefore, the  $f_{l,cc_0}^{sc}(k_c)$  is equal to  $f_{l,cc_0}^{sc,\theta}(k_c)$  that can be calculated with the complex-scaled wave functions  $\{\psi_{l,c}^{(c_0),\theta}(r)\}$ , as

$$f_{l,cc_0}^{sc,\theta}(k_c) = -\frac{2\mu_c}{\hbar^2 k_c k_{c_0}} e^{i\theta/2} \sum_{c'=1}^n \int_0^\infty dr \hat{j}_l(k_c r e^{i\theta}) V_{cc'}(r e^{i\theta}) \psi_{l,c}^{(c_0),\theta}(r). \quad (28)$$

Thus, we can obtain the full scattering amplitudes as

$$f_{l,cc_0}(k_c) = f_{l,cc_0}^{Born}(k_c) + f_{l,cc_0}^{sc}(k_c) \quad (29)$$

$$f_{l,cc_0}^{Born}(k_c) = -\frac{2\mu_c}{\hbar^2 k_c k_{c_0}} \int_0^\infty dr \hat{j}_l(k_c r) V_{cc_0}(r) \hat{j}_l(k_{c_0} r) \quad (30)$$

$$f_{l,cc_0}^{sc}(k_c) = f_{l,cc_0}^{sc,\theta}(k_c) \simeq -\frac{2\mu_c}{\hbar^2 k_c k_{c_0}} \sum_{c'=1}^n \sum_{j=1}^N t_{c',j}(\theta) b_{c',i}^\theta. \quad (31)$$

The  $f_{l,cc_0}^{sc,\theta}(k_c)$  can be obtained with the matrix elements  $\{b_{c',i}^\theta\}$  by using the Eqs. (23) and (26).

We summarize the essential points of the CS-WF at the end of this section. The first point is that the incoming part  $\hat{j}_l(k_{c_0} r)$  is separated from the scattered wave functions  $\{\psi_{l,c}^{(c_0),sc}(r)\}$  as shown in Eq. (18) and that only the scattered parts  $\{\psi_{l,c}^{(c_0)}(r)\}$  are complex-scaled. The complex scaling is used to make a non-square integrable function transformed to a square integrable

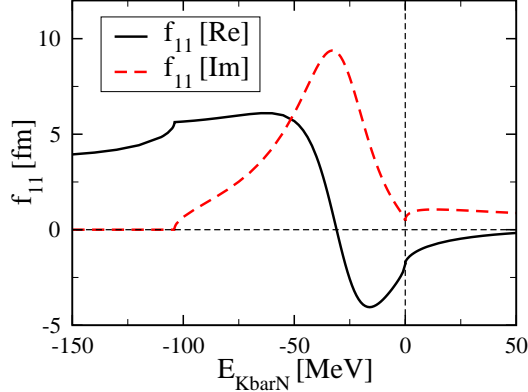


Figure 1: The  $\bar{K}N \rightarrow \bar{K}N$  scattering amplitude ( $f_{11}$ ) in the  $I = 0$  channel calculated with a phenomenological potential [1]. “ $E_{\bar{K}N}$ ” means the energy of the system measured from the  $\bar{K}N$  threshold.

one. If the full scattering wave function  $\Phi_{l,c}^{(c_0)}(r)$  is complex-scaled, it does not become a square-integrable function because of Riccati-Bessel function  $\hat{j}_l(k_{c_0}r)$  that contains both components of  $\exp\{\pm i(kr - \frac{l\pi}{2})\}$  in the asymptotic region. The second point is that we calculate the scattering amplitude with the complex-scaled function  $\psi_{l,c}^{(c_0),\theta}(r)$ , instead of the  $\psi_{l,c}^{(c_0)}(r)$  which is needed in usual calculation of the scattering amplitude. By the Cauchy’s theorem, the amplitude can be obtained with the  $\psi_{l,c}^{(c_0),\theta}(r)$  which is expressed with a square-integrable base. We note that the scattering amplitudes calculated in this way are independent of the scaling angle  $\theta$ .

In case of the semi-relativistic kinematics, the formula of scattering amplitudes is obtained by replacing the reduced mass  $\mu_c$  in Eqs. (30) and (31) with the reduced energy  $\tilde{\omega}_c$ . (See Appendix B.) The scattering amplitudes are calculated in the same way as the non-relativistic kinematics as explained above, by replacing the matrix elements of kinetic-energy term with those for the semi-relativistic kinematics. These matrix elements are given in Appendix C.

#### 2.4. Test of *ccCSM* for scattering amplitude

In this subsection, we test the CS-WF method by applying it to  $I = 0$   $\bar{K}N$ - $\pi\Sigma$  system, since it is the first time to apply this method to a meson-baryon system.

First, we use a phenomenological  $\bar{K}N$  potential [1]. Except for its energy independence, this potential is similar to our KSW-type potential; both are

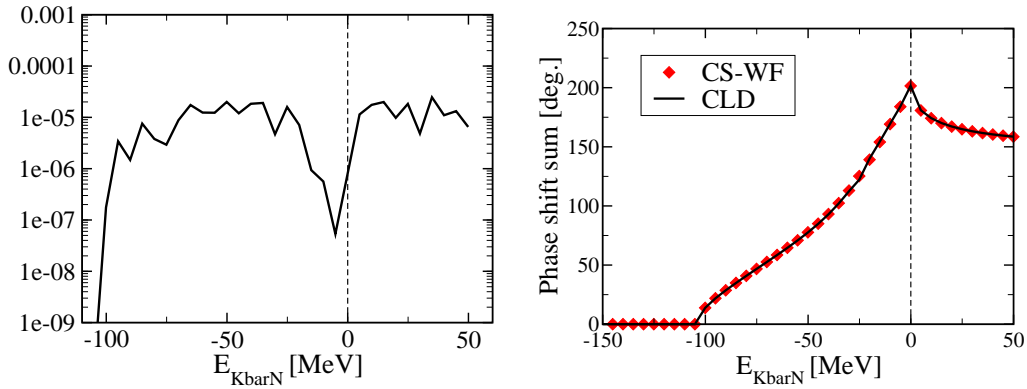


Figure 2: Test calculation of our method for the non-relativistic kinematics. (Left) Unitarity violation of the  $S$ -matrix. (Right) Comparison of the phase-shift sum between CS-WF (red diamond) and CLD (black line). Here, the  $I = 0$  channel is considered.

for coupled  $\bar{K}N$ - $\pi\Sigma$  channels, and given in a single Gaussian form in  $r$ -space. Therefore, we employ this potential for the first test.

Fig. 1 shows the  $\bar{K}N$  scattering amplitude obtained in the CS-WF method. In Ref. [1], the same Schrödinger equation is solved in the usual way and the resulting  $\bar{K}N$  amplitude is shown in Fig. 1 of Ref. [1]. By comparing them, one can see that our calculation reproduces the original result well. Two scattering lengths also agree well:  $-1.77 + i0.47$  fm in our calculation and  $-1.76 + i0.46$  fm in the original work.

Next, we test the CS-WF method with our energy-dependent potential. We use the NRv2 potential (Eq. (8)) in the NR kinematics case and the KSW-type potential (Eq. (3)) in the SR kinematics case. For both kinematics, we check violation of the unitarity of  $S$ -matrix;  $|\det S| - 1|$ . We calculate the  $S$ -matrix for the partial wave  $l$  with the scattering amplitude obtained by the CS-WF method. The  $S$ -matrix element for channels  $\alpha$  and  $\beta$  is related to the scattering amplitude as

$$S_{\beta,\alpha}^l = \delta_{\beta,\alpha} + 2ik_\alpha \sqrt{\frac{k_\beta/\mu_\beta}{k_\alpha/\mu_\alpha}} f_{\beta,\alpha}^l, \quad (32)$$

where  $k_\alpha$  is the wave number in the channel  $\alpha$ . The reduced masses  $\{\mu_\alpha\}$  in the NR case are replaced with the reduced energies  $\{\tilde{\omega}_\alpha\}$  in the SR case. As shown in the left panel of Fig. 2, in the NR case the magnitude of the unitarity violation is confirmed to be significantly small of the order of  $10^{-5}$

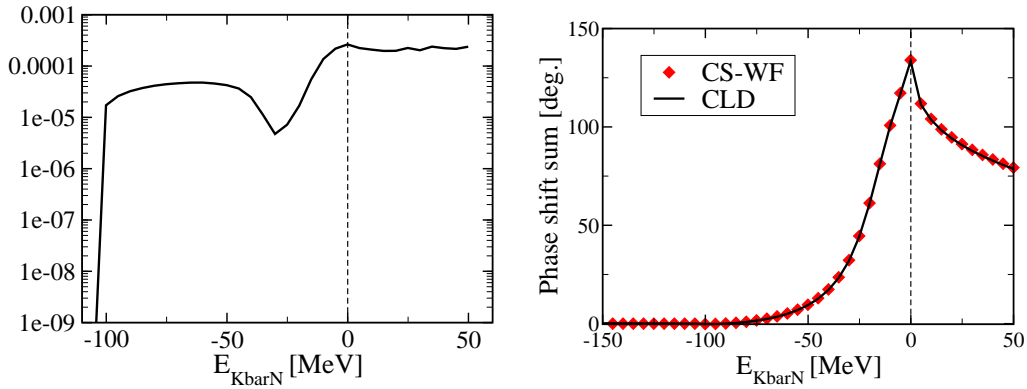


Figure 3: Same as Fig. 2, but for the semi-relativistic kinematics.

in  $\bar{K}N$  energy region of  $-100$  to  $50$  MeV. In the SR case, the violation is slightly larger than that in the NR case but still keeps the  $10^{-4}$  level as shown in Fig. 3, left panel. We consider that the larger violation is attributed to the numerical integration of kinetic-energy term in the SR calculation (see Appendix C).

We check also the phase-shift sum. We compare sum of the present phase shifts,  $\delta_{\bar{K}N} + \delta_{\pi\Sigma}$ , with that obtained by the continuum level density (CLD) method [32]. In the CLD method, the phase-shift sum is given by eigenvalues of the complex-scaled Hamiltonian, but the phase shift of each channel is not. Phase shift is extracted from the  $S$ -matrix (Eq. (32)) as

$$S = \begin{pmatrix} S_{11} & S_{12} \\ S_{21} & S_{22} \end{pmatrix} = \begin{pmatrix} \cos 2\epsilon e^{i\delta_1} & i \sin \epsilon e^{i(\delta_1+\delta_2)} \\ i \sin \epsilon e^{i(\delta_1+\delta_2)} & \cos 2\epsilon e^{i\delta_2} \end{pmatrix}, \quad (33)$$

where  $\delta_i$  is phase shift of channel  $i$  and  $\epsilon$  is a mixing parameter. As seen in the right panel of Figs. 2 and 3, the phase-shift sums calculated in the two methods agree with each other quite well in both the kinematics.

### 3. Results

We show results of our calculation for  $\bar{K}N-\pi Y$  system with the ccCSM. As mentioned in the section 2.1, we use our KSW-type potential and two kinds of its non-relativistic approximation. We use both the non-relativistic kinematics and the semi-relativistic kinematics. Hereafter we abbreviate non-relativistic and semi-relativistic as “NR” and “SR”, respectively. Natural combinations of potential types and kinematics are following:

Table 1: Range parameters for  $I = 0$   $\bar{K}N$ - $\pi\Sigma$  system.  $f_\pi = 110$  MeV case.  $d_{\bar{K}N, \bar{K}N}$  ( $d_{\pi\Sigma, \pi\Sigma}$ ) means the range parameter of Gaussian potential in  $\bar{K}N$ - $\bar{K}N$  ( $\pi\Sigma$ - $\pi\Sigma$ ) channel.  $a_{\bar{K}N(I=0)}$  is the  $I = 0$   $\bar{K}N$  scattering length calculated with given range parameters. “Martin” means that obtained by Martin’s analysis [29]. All quantities are in unit of fm.

Case	NRv1	NRv2	SR-A	SR-B	Martin
Kinematics	Non-rela.		Semi-rela.		—
Potential	NRv1	NRv2	KSW-type		—
$d_{\bar{K}N, \bar{K}N}$	0.440	0.438	0.499	0.369	—
$d_{\pi\Sigma, \pi\Sigma}$	0.605	0.636	0.712	0.348	—
Re $a_{\bar{K}N(I=0)}$	-1.701	-1.700	-1.700	-1.696	-1.70
Im $a_{\bar{K}N(I=0)}$	0.681	0.681	0.681	0.681	0.68

- Case NRv1 One of non-relativistic approximated KSW-type potentials (Eq. (7)), NRv1, with the non-relativistic kinematics.
- Case NRv2 The other non-relativistic approximated KSW-type potentials (Eq. (8)), NRv2, with the non-relativistic kinematics.
- Case SR The KSW-type potential (Eq. (3)) with the semi-relativistic kinematics.

We consider  $f_\pi$  in the KSW-type potential as a parameter in our model. In the present study, it is varied around the physical values of  $f_\pi \simeq 93$  MeV and  $f_K \simeq 110$  MeV. We examine four cases of  $f_\pi = 90, 100, 110$  and  $120$  MeV. The results shown in the following sections are obtained with  $f_\pi = 110$  MeV if the  $f_\pi$  value is not specified.

### 3.1. Scattering amplitude of $I = 0$ $\bar{K}N$ - $\pi\Sigma$ system

First, we determine the range parameters of Gaussian functions,  $\{d_{\alpha\beta}^{I=0}\}$ , in the meson-baryon potentials defined in Eqs. (3), (7) and (8). In the present study, with an assumption of  $d_{\bar{K}N, \pi\Sigma} = d_{\pi\Sigma, \bar{K}N} = (d_{\bar{K}N, \bar{K}N} + d_{\pi\Sigma, \pi\Sigma})/2$ , we search for the two of the range parameters,  $d_{\bar{K}N, \bar{K}N}$  and  $d_{\pi\Sigma, \pi\Sigma}$ , so as to reproduce the complex value of  $\bar{K}N$  scattering length with  $I = 0$  which was obtained by Martin’s analysis;  $a_{\bar{K}N(I=0)} = -1.70 + i0.68$  fm [29]. For all combinations of kinematics and meson-baryon potential, we can find the range parameters which reproduce the Martin’s value. The determined range parameters and the resulting  $\bar{K}N$  scattering length for  $f_\pi = 110$  MeV case are listed in Table 1. It should be noted that in the semi-relativistic case we

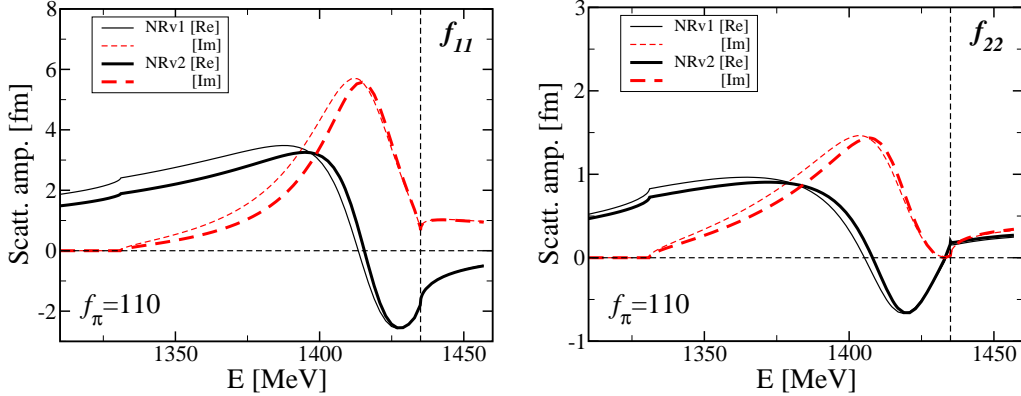


Figure 4:  $I = 0$  scattering amplitudes for NRv1 and NRv2 cases with  $f_\pi = 110$  MeV. The scattering amplitudes of NRv1 (NRv2) are shown with thin (bold) line. The real (imaginary) part of scattering amplitude is drawn with a black-solid (red-dashed) line. Left (right) panel shows  $\bar{K}N$  ( $\pi\Sigma$ ) scattering amplitude. Vertical dashed line means the  $\bar{K}N$  threshold.

find two sets of the range parameters as shown on the right two columns in the table. Hereafter, we denote them as “SR-A” and “SR-B”, respectively. Also in cases of other  $f_\pi$  values, we determine the range parameters as given in Table D.5.

Using the meson-baryon potentials with these range parameters, we calculate the scattering amplitude in the  $I = 0$  channel. Figs. 4 - 6 show the  $\bar{K}N$  and  $\pi\Sigma$  scattering amplitudes for  $f_\pi = 110$  MeV. As seen in Figs. 4 and 5, the NR and SR-A give quantitatively the same scattering amplitudes. Let us see the  $I = 0$  scattering amplitudes in more detail. In two non-relativistic cases NRv1 and NRv2, there is almost no difference between their scattering amplitudes. Compared with these NR cases, magnitude of scattering amplitudes becomes larger near the  $\pi\Sigma$  threshold in a semi-relativistic case SR-A, though near the  $\bar{K}N$  threshold the scattering amplitudes of both cases are the same. Fig. 6 is a result of the other semi-relativistic case SR-B. The global distribution of  $\bar{K}N$  scattering amplitude is quite similar to the NR result. However, the  $\pi\Sigma$  scattering amplitude is very different from that of NR.

We investigate the  $f_\pi$  dependence of the scattering amplitude. Figs. 7 - 9 show the scattering amplitudes of the NRv2, SR-A and SR-B cases, respectively, in which  $f_\pi$  is varied from 90 to 120 MeV. In the NR case, it is found that the scattering amplitude depends strongly on the  $f_\pi$  value,

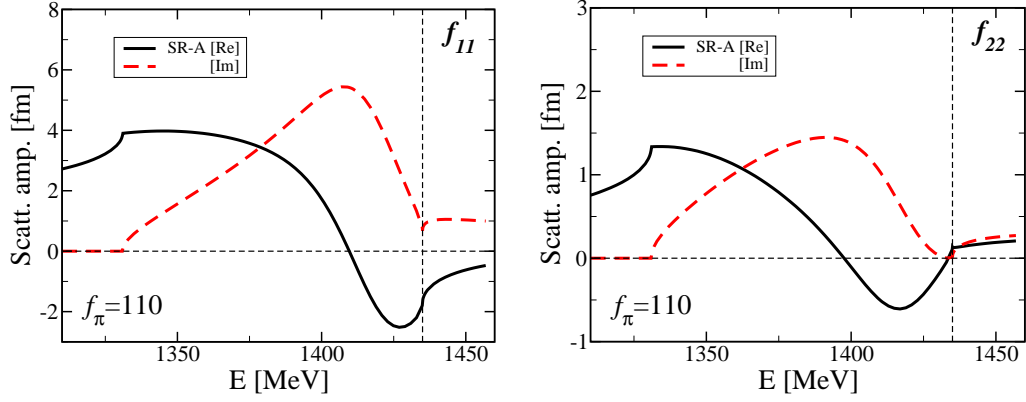


Figure 5:  $I = 0$  scattering amplitudes for SR-A case with  $f_\pi = 110$  MeV. Similar to Fig. 4.

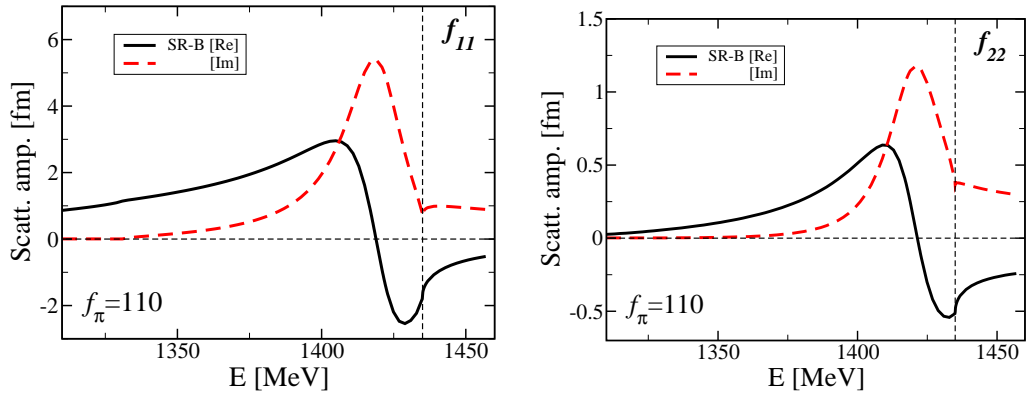


Figure 6:  $I = 0$  scattering amplitudes for SR-B case with  $f_\pi = 110$  MeV. Similar to Fig. 4.

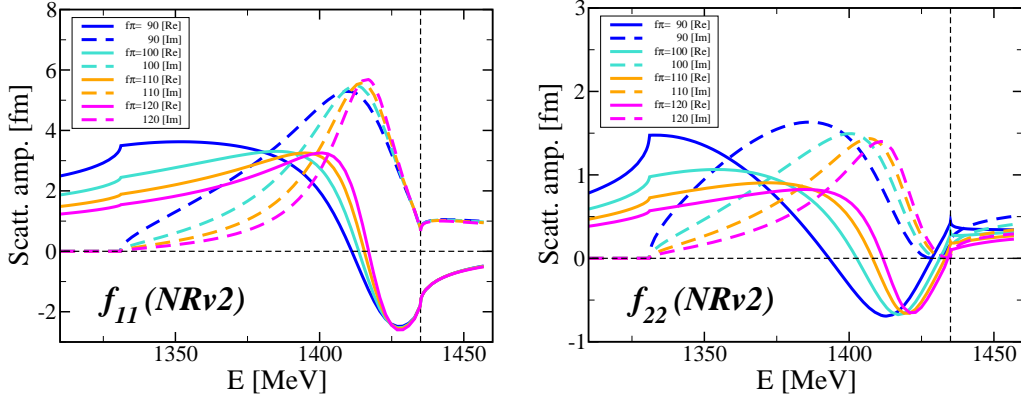


Figure 7:  $I = 0$  scattering amplitudes for NRv2 case, calculated with various  $f_\pi$  values. Blue, light blue, orange and magenta lines correspond to  $f_\pi=90, 100, 110$  and  $120$  MeV, respectively. Solid (dashed) line indicates the real (imaginary) part of scattering amplitude. Left (right) panel shows  $\bar{K}N$  ( $\pi\Sigma$ ) scattering amplitude.

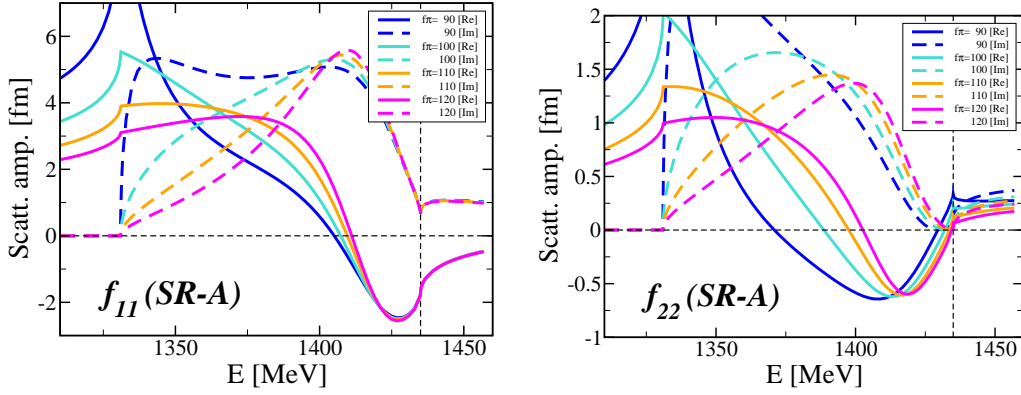


Figure 8:  $I = 0$  scattering amplitudes for SR-A case, calculated with various  $f_\pi$  values. Similar to Fig. 7.

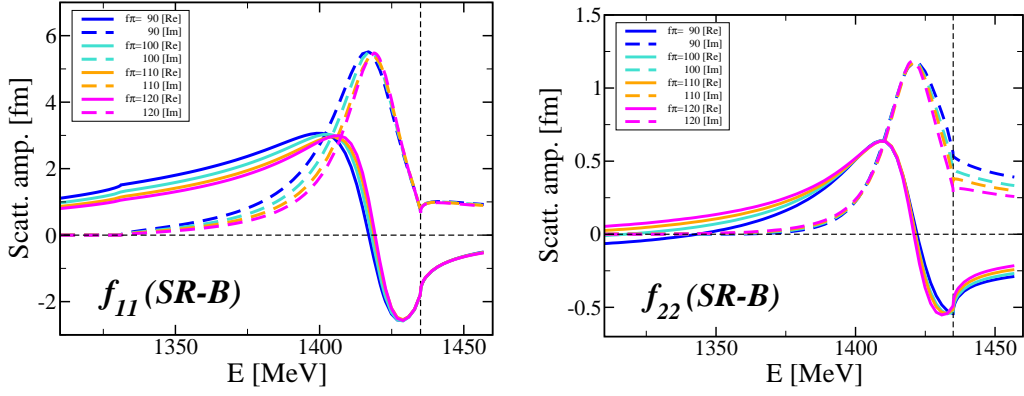


Figure 9:  $I = 0$  scattering amplitudes for SR-B case, calculated with various  $f_\pi$  values. Similar to Fig. 7.

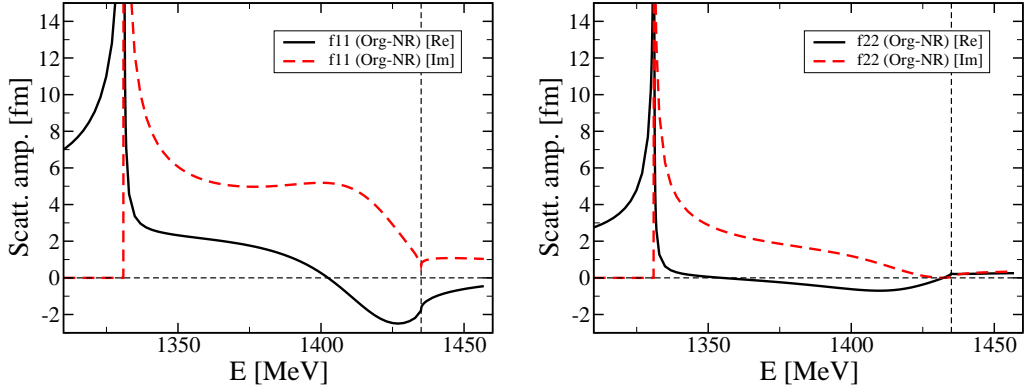


Figure 10:  $I = 0$  scattering amplitudes calculated with the KSW-type potential used in NR kinematics.  $f_\pi = 90$  MeV. Similar to Fig. 4. The  $\bar{K}N$  scattering length calculated is  $a_{\bar{K}N(I=0)} = -1.709 + i0.679$  fm when the range parameters are  $(d_{\bar{K}N, \bar{K}N}, d_{\pi\Sigma, \pi\Sigma}) = (0.593, 0.541)$  fm.

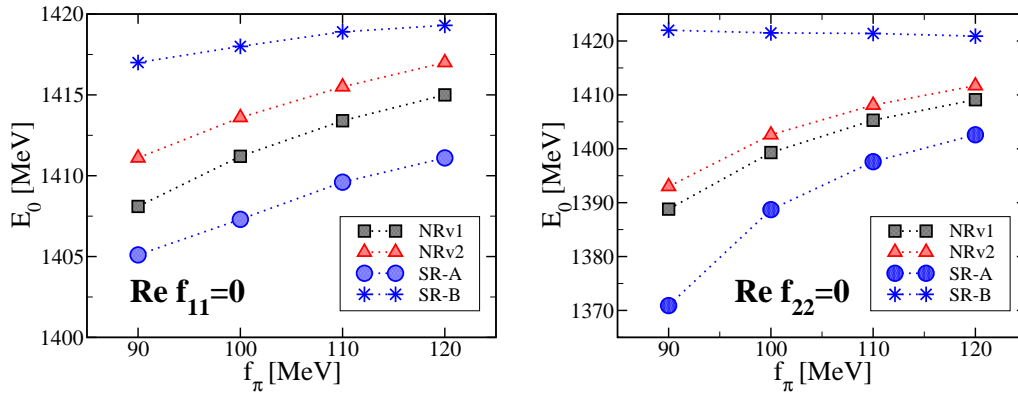


Figure 11: Resonance energies estimated from scattering amplitudes.  $f_\pi = 90 \sim 120$  MeV (Left)  $E_0(\bar{K}N)$  obtained from the  $\bar{K}N$  scattering amplitude. (Right)  $E_0(\pi\Sigma)$  obtained from the  $\pi\Sigma$  one. Black square and red triangle mean NRv1 and NRv2, respectively. Blue circle and asterisk mean SR-A and SR-B, respectively.

especially near the  $\pi\Sigma$  threshold as shown in Fig. 7. The SR-A case has a similar tendency as shown in Fig. 8. On the other hand, in the SR-B case which is the other semi-relativistic case, the amplitudes don't depend on the  $f_\pi$  value so much. (See Fig. 9.) In all cases, the amplitudes far below  $\bar{K}N$  threshold tend to be less attractive at larger value of  $f_\pi$ .

For instruction, we have examined a case where kinematics and potential are mismatched. When the KSW-type potential is used under the non-relativistic kinematics, the scattering amplitude behaves singularly as shown in Fig. 10, which is the most typical case ( $f_\pi = 90$  MeV). Both the  $\bar{K}N$  and  $\pi\Sigma$  scattering amplitudes are singular at the  $\pi\Sigma$  threshold. By investigating the relation between scattering length  $a_{\pi\Sigma}$  and effective range  $r_e$  in the  $\pi\Sigma$  channel, it is found that a virtual state is generated in this case. Obtained values of  $(a_{\pi\Sigma}, r_e)$  are  $(61, -6.3)$  fm. According to Appendix A in Ref. [33],  $(a_{\pi\Sigma}, r_e)$  satisfying the condition  $-a_{\pi\Sigma}/2 < r_e$  is an indication of the existence of a virtual state without decay width. This virtual state causes such a singularity in scattering amplitudes. We consider that the KSW-type potential should be used under the relativistic kinematics (semi-relativistic, at least) since the flux factor involved in this potential is based on relativistic kinematics.

In all cases, the resonance structure is found in the  $\bar{K}N$  and  $\pi\Sigma$  scattering amplitudes below the  $\bar{K}N$  threshold. We estimate the resonance energies  $E_0(\bar{K}N)$  and  $E_0(\pi\Sigma)$  from the scattering amplitudes  $f_{\bar{K}N}$  and  $f_{\pi\Sigma}$  by putting

Table 2: Pole position of the  $I = 0$   $\bar{K}N$ - $\pi\Sigma$  system and the meson-baryon distance in the pole state.  $(E_R, -\Gamma/2)$  indicates the complex energy of the resonance pole.  $B_{\bar{K}N}$  means the binding energy that is the  $E_R$  measured from the  $\bar{K}N$  threshold. The unit of these energies is MeV.  $\sqrt{\langle r^2 \rangle_{\bar{K}N}}$ ,  $\sqrt{\langle r^2 \rangle_{\pi\Sigma}}$  and  $\sqrt{\langle r^2 \rangle_{\bar{K}N+\pi\Sigma}}$  indicate the meson-baryon mean distance of  $\bar{K}N$ ,  $\pi\Sigma$  and total components, respectively. These values are given in unit of fm.  $f_\pi = 110$  MeV case.

Case	NRv1	NRv2	SR-A	SR-B
Kinematics	Non-rela.		Semi-rela.	
Potential	NRv1	NRv2	KSW-type	
$E_R$	1416.6	1417.8	1419.5	1420.0
$\Gamma/2$	19.5	16.6	25.0	12.8
$(B_{\bar{K}N})$	(18.4)	(17.2)	(15.5)	(15.0)
$\sqrt{\langle r^2 \rangle_{\bar{K}N}}$	$1.31 - 0.37i$	$1.37 - 0.37i$	$1.22 - 0.47i$	$1.18 - 0.49i$
$\sqrt{\langle r^2 \rangle_{\pi\Sigma}}$	$0.39 + 0.05i$	$0.37 + 0.04i$	$0.13 + 0.05i$	$0.11 - 0.06i$
$\sqrt{\langle r^2 \rangle_{\bar{K}N+\pi\Sigma}}$	$1.36 - 0.34i$	$1.42 - 0.34i$	$1.22 - 0.47i$	$1.18 - 0.49i$

the conditions on  $\text{Re } f_{\bar{K}N}(E_0(\bar{K}N)) = 0$  and  $\text{Re } f_{\pi\Sigma}(E_0(\pi\Sigma)) = 0$ , respectively. For various  $f_\pi$ ,  $E_0(\bar{K}N)$  and  $E_0(\pi\Sigma)$  are shown in Fig. 11. In the non-relativistic kinematics the estimated energies are not so different between NRv1 and NRv2, since the scattering amplitudes are almost same in these cases as shown in Fig. 4. In the semi-relativistic kinematics, there are two sets of the parameters, SR-A and SR-B, as explained before. Since these two sets give quite different scattering amplitudes as shown in Figs. 8 and 9, the resonance energies are also different between them. Compared with the NR cases,  $E_0(\bar{K}N)$  and  $E_0(\pi\Sigma)$  in SR-A are smaller, while those in SR-B are larger. In particular, the  $f_\pi$  dependence of  $E_0(\pi\Sigma)$  in SR-B is quite different from the NR cases, while that in SR-A is rather strong but qualitatively similar to them. In SR-B, the resonance energies (especially  $E_0(\pi\Sigma)$ ) are quite stable for  $f_\pi$  value and remain to be around 1420 MeV.

### 3.2. Property of the $I = 0$ $\bar{K}N$ - $\pi\Sigma$ resonant state

Using the meson-baryon potential determined in the previous section, we investigate the resonance in the  $I = 0$   $\bar{K}N$ - $\pi\Sigma$  system. In practice, we search poles on the complex-energy plane with the usual complex scaling method as explained in the section 2.2. In all NR and SR cases, one pole is clearly

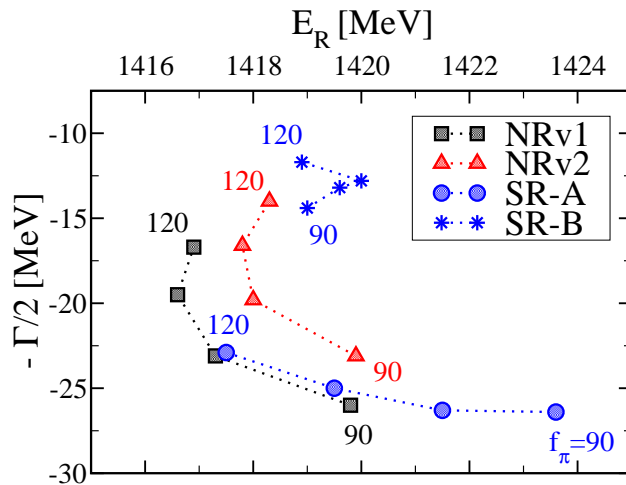


Figure 12:  $I = 0$  pole in the complex-energy plane, calculated with NRv1, NRv2, and SR for various  $f_\pi$  values. Black square and red triangle mean NRv1 and NRv2, respectively. Blue circle and asterisk mean SR-A and SR-B, respectively. The number shown in the panel indicates the  $f_\pi$  value which increases continuously from 90 to 120 along the connected dashed line in each case.

found.<sup>2</sup> We denote the complex energy of a resonance pole as  $(E_R, -\Gamma/2)$ . The found poles for the case  $f_\pi = 110$  MeV are shown in Table 2. The real part of energy  $E_R$  is well determined to be about 1420 MeV, independently of kinematics and potential types. The imaginary part of energy  $\Gamma/2$  depends on the kinematics. The  $\Gamma/2$  is about 18 MeV in the NR. In the SR, it should be noted that the two potentials give quite different values;  $\Gamma/2 \simeq 25$  MeV in the SR-A and  $\Gamma/2 \simeq 13$  MeV in the SR-B.

Fig. 12 shows the pole positions of all cases when the  $f_\pi$  value is varied from 90 MeV to 120 MeV. In the NR cases,  $E_R$  is stable for  $f_\pi$  and is 1417-1420 MeV, but  $\Gamma/2$  is ranging from 14 MeV to 26 MeV. In the SR cases, the poles of SR-A and those of SR-B show completely different behavior for the variation of  $f_\pi$ . In the SR-A case, the pole moves widely in the  $E_R$  direction from 1417 MeV to 1424 MeV, while keeping  $\Gamma/2$  to be about 25 MeV. On the other hand, in the SR-B case the poles are found to distribute in compact region. The pole position  $(E_R, -\Gamma/2)$  is determined with small deviation;  $(1419.5 \pm 1, -13 \pm 2)$  MeV. From these results, it seems that the real energy

<sup>2</sup> Preceding studies based on the chiral SU(3) theory reported that there exist two poles in the  $I = 0$  channel [18, 19] We will discuss a signature of another pole later.

of the pole is rather determined well, compared to the imaginary energy. The imaginary energy of the pole indicates a half width decaying to  $\pi\Sigma$ . In our study we have a constraint for  $\bar{K}N$  channel but no constraint for  $\pi\Sigma$  channel. We consider that the large deviation of  $\Gamma/2$  is due to the lack of constraint condition for  $\pi\Sigma$  channel.

Here, we mention the difference between the SR-A and SR-B which are two solutions of the semi-relativistic case. Observing the pole behavior for the  $f_\pi$  variation in Fig. 12, we notice that the pole behavior of the SR-A is qualitatively the same as that of the NR cases, while the SR-B shows completely different behavior from the NR cases. In the SR-A case, when the  $f_\pi$  decreases, the pole moves with  $E_R$  and  $\Gamma/2$  decreasing in the same way as the NR cases. However, in the SR-B case the pole moves quite in a different way. Taking into account also results of the scattering amplitude as given in the previous section, we consider that *a semi-relativistic solution, SR-A, can be regarded as a kind of semi-relativistic version of the non-relativistic solutions (NRv1 and NRv2)*, because it has qualitatively the similar properties to the NR's. The other one, the SR-B, is a unique solution to the semi-relativistic kinematics, which has completely different properties from the NR's.

We have investigated another pole which is expected to exist, because many studies of the  $I = 0$   $\bar{K}N$ - $\pi\Sigma$  system reported that this system has a double pole structure when an energy-dependent chiral SU(3) potential is used as we use [18, 19]; The higher pole state is slightly below the  $\bar{K}N$  threshold and with small width, while the lower one is far below the  $\bar{K}N$  threshold and with large width. (For instance, the former is around (1432, -17) MeV and the latter is around (1400, -80) MeV [19].) In our study, certainly we have found self-consistent solutions which seem to indicate a lower pole of the two poles; In the non-relativistic kinematics, it is found at the complex energy ( $\sim 1360, -90 \sim -40$ ) MeV in case of NRv2, and in the semi-relativistic kinematics it is around (1350  $\sim$  1390, -100  $\sim$  -30) in case of SR-A, though no self-consistent solutions are found in the deep binding region in case of SR-B. In the previous subsection scattering amplitudes of the NRv2 and SR-A are shown in Figs. 4 and 5, respectively. These scattering amplitudes are found to have qualitatively a similar feature to the amplitudes obtained in the former studies [19, 33] which involve the double pole structure. With this fact, the self-consistent solution of the NRv2 and SR-A is expected to be a lower pole. However, the position of these poles, in particular the imaginary energy, rather depends on the scaling angle  $\theta$ . In the NRv2 case, the separation of the pole from continuum states indicated

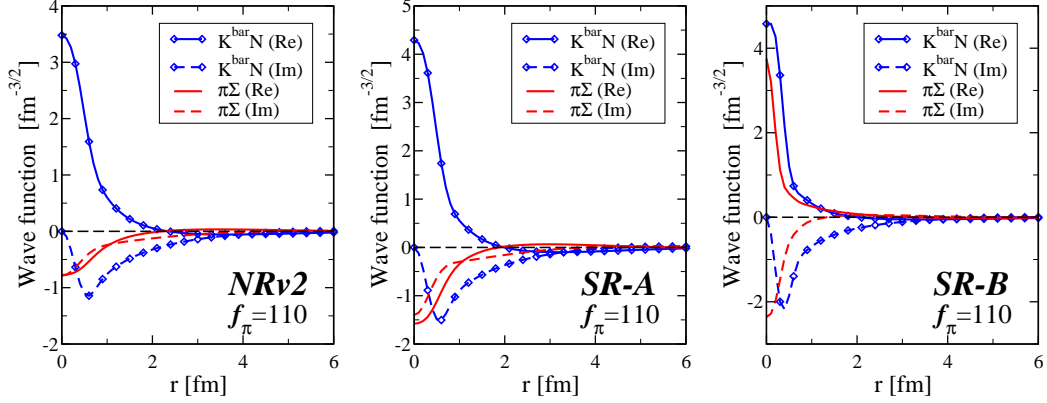


Figure 13: Complex-scaled wave function of each component in the  $I = 0$  pole state at  $\theta = 30^\circ$ . We choose a phase such that the  $\bar{K}N$  wave function becomes real at  $r = 0$ . Blue (red) lines show  $\bar{K}N$  ( $\pi\Sigma$ ) wave function, whose real (imaginary) part is drawn with solid (dashed) lines. Left: NRv2, middle: SR-A, right: SR-B.  $f_\pi = 110$  MeV case.

by the  $2\theta$ -line on the complex-energy plane seems insufficient. We consider that these difficulties to specify the pole position are due to the limitation of the numerical accuracy. When poles have large decay width compared to excitation energy, it is known empirically that such poles are difficult to be found by the CSM with Gaussian base, since the spatial oscillation of the complex-scaled wave function is not well described with them. Therefore, we cannot conclude yet that the double pole structure is confirmed in the present our analysis. We need more investigation of the lower pole.

We are interested in the inertial structure of  $\Lambda(1405)$ , which has been investigated theoretically in various ways [34, 35, 36]. We check the wave function of the pole state obtained in our ccCSM calculation. Fig. 13 shows complex-scaled wave functions of each component with the scaling angle  $\theta = 30^\circ$ . Here, the wave functions are multiplied by an appropriate phase factor so that the  $\bar{K}N$  wave function becomes real at  $r = 0$ . Without this phase factor, the complex-scaled wave function of  $\bar{K}N$ - $\pi\Sigma$  is normalized using Eq. (12). Both of  $\bar{K}N$  and  $\pi\Sigma$  wave functions are confirmed to be well localized. It is noted that localization of the  $\pi\Sigma$  component is due to the complex scaling, in spite that the state is above  $\pi\Sigma$  threshold. In these wave functions, it can be confirmed also that a semi-relativistic case SR-B shows especially different nature from other cases. The SR-B wave function is much compact and its real part of  $\pi\Sigma$  component has the opposite phase to other cases. The wave function of the other semi-relativistic case SR-A is similar to that of a

non-relativistic one NRv2.

The mean distance between meson and baryon in the resonant state is calculated as

$$\langle \hat{r}_{MB}^2 \rangle = \langle \tilde{\Phi}_\theta | \hat{r}_{MB,\theta}^2 | \Phi_\theta \rangle, \quad (34)$$

where  $\hat{r}_{MB} = \hat{r}_{\text{Meson}} - \hat{r}_{\text{Baryon}}$  and  $\Phi_\theta$  means the complex-scaled wave function of the resonance pole. It should be noted that the matrix elements of resonant state are obtained independently of  $\theta$  because the properties of the resonant wave functions are uniquely determined as the Gamow states [37]. The expectation value calculated with Eq. (34) is inevitably a complex number because the resonant state is treated as a Gamow state in our framework. Therefore, the root-mean square distance,  $\sqrt{\langle \hat{r}_{MB}^2 \rangle}$ , is also a complex number. Certainly its physical meaning is still unclear, but we show this quantity as a reference for the size. We believe that it is useful for us to get a feeling of the size of the system. Indeed, since the imaginary part of the obtained complex mean distance is smaller than its real part as will be shown later, we consider that the real part can be regarded as a mean distance with a physical meaning [37].

If such an interpretation for the complex-valued distance calculated within the ccCSM is accepted, the mean distance between meson and baryon is  $\sim 1.4$  fm in NR kinematics and  $\sim 1.2$  fm in SR kinematics when  $f_\pi = 110$  MeV, as shown in Table 2. Those for other  $f_\pi$  values are given in Table D.6. In both semi-relativistic cases of SR-A and SR-B, the mean distance has small  $f_\pi$  dependence, remaining about 1.2 fm. In the NR case it depends on the  $f_\pi$  value similarly to the pole position, but it increases slightly from 1.2 fm to 1.4 fm when  $f_\pi$  increases from 90 MeV to 120 MeV. Thus, it is found that the mean distance is almost the same in both two kinematics. As for the imaginary part of the complex-valued distance, it is certainly small value of 0.5 fm at most.

Compared to results of other studies, the size obtained in our calculation seems rather small, even if the modulus of  $\sqrt{\langle \hat{r}_{MB}^2 \rangle}$  is regarded as a mean distance between meson and baryon in the  $I = 0$  system. For example, according to the study using a chiral SU(3)-based potential, the size is obtained as 1.9 fm with 12 MeV binding energy of  $\bar{K}N$  ( $M = 1423$  MeV) [7]. It is considered that the difference of sizes between two calculations is mainly caused by different definition of the resonant state. In the previous study, the state is treated as a  $\bar{K}N$  bound state, as a result of elimination of

$\pi\Sigma$  channel and perturbative treatment of the imaginary part of potential. On the other hand, the resonant state is a Gamow state in the current study since the complex scaling method imposes the correct outgoing boundary condition on a solution implicitly.

### 3.3. Comparison with other studies of $I = 0$ $\bar{K}N$ - $\pi\Sigma$ scattering amplitude

There are many studies of the  $I = 0$   $\bar{K}N$ - $\pi\Sigma$  scattering amplitude. Here, we compare our result mainly with that of Ref. [33], because some of their models are constructed under the same condition as our study: Their models “A1” and “B E-dep” employ the Weinberg-Tomozawa term as an interaction kernel and are constrained with the  $I = 0$   $\bar{K}N$  scattering length. Their amplitudes are calculated under the relativistic kinematics. Therefore, their results of models A1 and B E-dep can be directly compared with those of the SR case of our study.

Similarly to Ref. [33], we set the value of  $f_\pi$  to be 92.4 MeV in our SR calculation. Also with this  $f_\pi$  value, we find two parameter sets which correspond to SR-A and SR-B, while in Ref. [33] a single solution is reported for each model. Fig. 14 shows the scattering amplitudes of both SR-A and SR-B. Compared with the scattering amplitudes of model A1 shown in Fig. 1 in their paper, both of SR-A and SR-B are found to give different amplitudes from them. In a case of SR-A, both scattering amplitudes of  $\bar{K}N$  and  $\pi\Sigma$  behave similarly to those of model A1 near the  $\bar{K}N$  threshold. However, far from the  $\bar{K}N$  threshold they are quite different from the amplitudes of model A1. In the other case of SR-B, the  $\bar{K}N$  amplitude is almost the same as that of model A1, whereas the  $\pi\Sigma$  one is completely different from that of model A1. As for resonance poles, we find a pole at (1423.1, -26.4) MeV and (1419.4, -14.1) MeV in SR-A and SR-B, respectively. It is known that the models in Ref. [33] give double pole structure. The higher pole of them are at (1422, -16) MeV in the model A1 and (1422, -22) MeV in the model B E-dep. They are rather close to the poles found in the SR-B and SR-A, respectively.

We notice that the interaction kernel is slightly different between our study and Ref. [33]. The energy dependence of the interaction kernel is just the sum of meson energies such as  $\omega_\alpha + \omega_\beta$  which is involved in the pseudo-potential  $\hat{V}_{MB}^{SR}$  as shown in Eq. (3). On the other hand, it is given as  $(2\sqrt{s} - M_\alpha - M_\beta)\sqrt{\frac{E_\alpha + M_\alpha}{2M_\alpha}}\sqrt{\frac{E_\beta + M_\beta}{2M_\beta}}$  in their study. Compared with our interaction kernel, the relativistic  $q^2$  correction and the non-static effect of

baryons are taken into account by the first term and the additional square-root terms, respectively. We investigate the influence of interaction kernels with different energy dependence. Here, we make a pseudo-potential from their interaction kernel, following our ansatz that a relativistic flux factor is used and a Gaussian form is assumed:

$$\hat{V}_{MB}^{Ref. [33]} = \sum_{\alpha, \beta} -\frac{C_{\alpha\beta}^I}{8f_\pi^2} (2\sqrt{s} - M_\alpha - M_\beta) \sqrt{\frac{E_\alpha + M_\alpha}{2M_\alpha}} \sqrt{\frac{E_\beta + M_\beta}{2M_\beta}} \times \sqrt{\frac{M_\alpha M_\beta}{s \tilde{\omega}_\alpha \tilde{\omega}_\beta}} g_{\alpha\beta}^I(r) |\alpha\rangle\langle\beta|. \quad (35)$$

Scattering amplitudes calculated with this pseudo-potential are drawn with thick line in Fig. 14. Two sets of range parameters are found also for this potential. It is confirmed that the scattering amplitudes differ slightly from those obtained with the pseudo-potential  $\hat{V}_{MB}^{SR}$ . In the SR-A, in particular, the amplitudes near the  $\pi\Sigma$  threshold are suppressed, compared with those with  $\hat{V}_{MB}^{SR}$ . However, they are still larger than the scattering amplitudes of the model A1 in Ref. [33]. Therefore, the difference between our result and Ref. [33] is partially attributed to the difference of the interaction kernel. We note that in the SR-B the scattering amplitudes are not so different between two interaction kernels, since the magnitude of amplitudes near  $\pi\Sigma$  threshold is rather small compared with the SR-A model. The small scattering amplitudes may be related to the fact that the SR-B has rather small range parameters compared with other models, as listed in Tables 1 and D.5.

In addition, we consider that the ansatz of a relativistic flux factor and/or the assumption of Gaussian form may also contribute to such a difference. We comment on the latter ingredient. The Gaussian form possesses such a nature potentially that it enhances the magnitude of a scattering amplitude far below a threshold. It is easily confirmed by Born approximation that the  $s$ -wave scattering amplitude for single-range Gaussian potentials diverges as  $|E|^{-1} \exp [c|E|]$  when  $E \rightarrow -\infty$  [38]. (The number  $c$  is a positive constant.) Indeed, as mentioned before, the scattering amplitudes of SR-A with our potential  $\hat{V}_{MB}^{SR}$  has large magnitude near the  $\pi\Sigma$  threshold (namely far below the  $\bar{K}N$  threshold) compared with the model A1 of Ref. [33]. The similar tendency can be seen in the comparison with another study. In Ref. [19] only the WT term is used as well but the constraint condition for the scattering

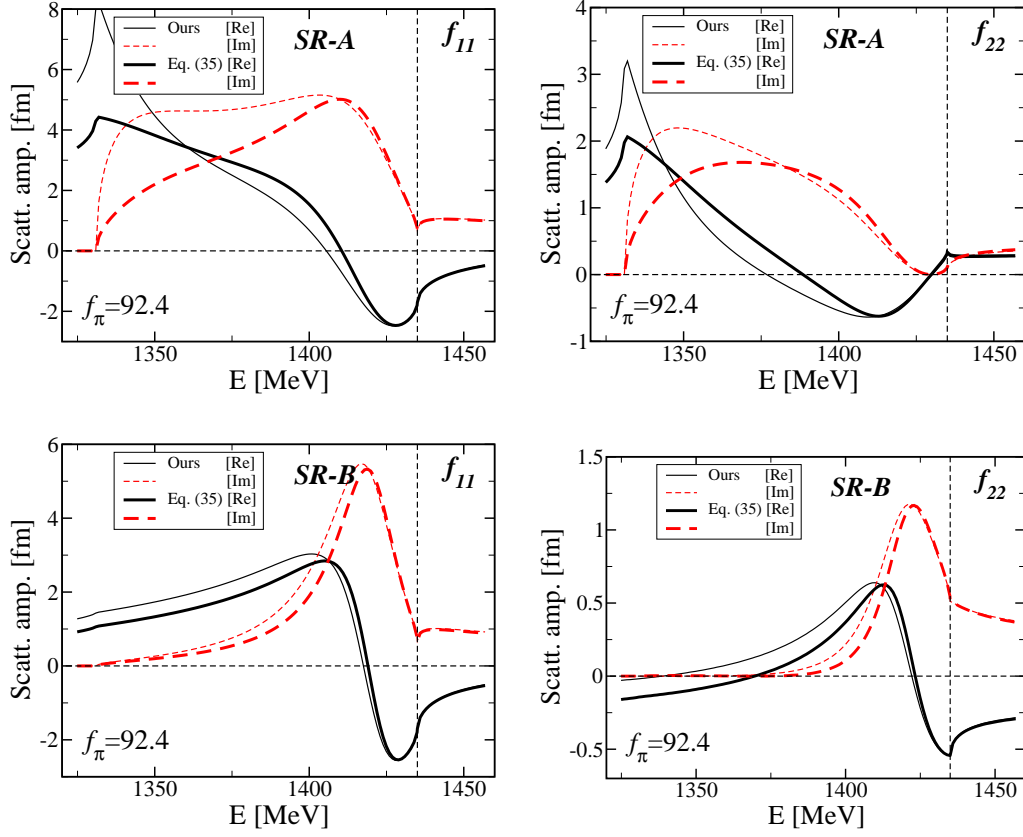


Figure 14:  $I = 0$  scattering amplitudes calculated with different interaction kernels. The thick (thin) line indicates the amplitude obtained with the pseudo-potential Eq. (35) (Eq. (3)). Left (right) panels show  $\bar{K}N$  ( $\pi\Sigma$ ) scattering amplitude. Two types of scattering amplitudes, SR-A and SR-B, are given in upper and lower panels, respectively.  $f_\pi = 92.4$  MeV.

amplitude is different from ours. Anyway, when the amplitudes shown in Fig. 4 in their paper are compared with our ones<sup>3</sup> of SR-A calculated with the above  $\hat{V}_{MB}^{Ref. [33]}$  using the same  $f_\pi$  as that of Ref. [19] (106.95 MeV), it is confirmed that the magnitude of their scattering amplitudes are significantly smaller near the  $\pi\Sigma$  threshold. In both the model A1 of Refs. [33] and the model of Ref. [19], the dimensional regularization is used to obtain a finite result. On the other hand, it can be said in the present study that such a regularization is realized by using the Gaussian-form potential. The different regularization scheme causes the different extrapolation of the scattering amplitudes to the subthreshold region. This is considered to be a possible reason of the difference between our result and results of other studies.

#### 3.4. $I = 1$ $\bar{K}N$ - $\pi\Sigma$ - $\pi\Lambda$ system

We make the same investigation on the isospin  $I = 1$  sector which has three channels of  $\bar{K}N$ ,  $\pi\Sigma$  and  $\pi\Lambda$ . In our model of the Gaussian-form potential, there are six range parameters in this sector. However, two of them,  $d_{\pi\Lambda, \pi\Sigma}$  and  $d_{\pi\Lambda, \pi\Lambda}$ , give no contribution to the result, since the potential strength of these channels are forced to be zero due to the SU(3) algebra which is involved in the Weinberg-Tomozawa term of effective chiral SU(3) Lagrangian. (See  $C^{(I=1)}$  in Eq. (6).) Since we assume  $d_{\bar{K}N, \pi\Sigma} = (d_{\bar{K}N, \bar{K}N} + d_{\pi\Sigma, \pi\Sigma})/2$  similarly to the  $I = 0$  case, three range parameters,  $d_{\bar{K}N, \bar{K}N}$ ,  $d_{\pi\Sigma, \pi\Sigma}$  and  $d_{\bar{K}N, \pi\Lambda}$ , are unknown parameters to be determined.

Similarly to the  $I = 0$  case, we constrain the range parameters in the potential by the Martin's value of the  $I = 1$   $\bar{K}N$  scattering length;  $a_{\bar{K}N(I=1)} = 0.37 + i0.60$  fm [29]. However, the three unknown parameters can't be determined by only the complex value of  $a_{\bar{K}N(I=1)}$ . Here, we reduce the number of unknown parameters by referring the following two facts: 1. In studies with chiral unitary model, isospin symmetric subtraction constants have been often assumed and succeeded to reproduce various physical quantities [39]. 2. In a separable potential used in Faddeev-AGS calculation of  $\bar{K}NN$ - $\pi YN$  [5], the cut-off parameter for the  $\bar{K}N$  channel is not so different between  $I = 0$  and  $I = 1$  sector. Based on these facts, we examine three conditions as follows:

---

<sup>3</sup>This scattering amplitude has a similar shape with that of  $f_\pi = 120$  MeV case shown in Fig. 8.

Table 3: Range parameters for the  $I = 1$   $\bar{K}N$ - $\pi\Sigma$ - $\pi\Lambda$  system with non-relativistic and semi-relativistic kinematics (NRv2 and SR-A).  $f_\pi = 110$  MeV. Same as Table 1. “Condition” is explained in the text.

Case	NRv2			SR-A		
Kinematics	Non-rela.			Semi-rela.		
Potential	NRv2			KSW-type		
Condition	(a)	(b)	(c)	(a)	(b)	(c)
$d_{\bar{K}N, \bar{K}N}$	0.438	0.438	0.438	0.499	0.499	0.499
$d_{\pi\Sigma, \pi\Sigma}$	0.159	0.636	0.636	0.261	0.712	0.712
$d_{\bar{K}N, \pi\Lambda}$	0.221	0.301	0.445	0.282	0.354	0.467
Re $a_{\bar{K}N(I=1)}$	0.376	0.372	0.657	0.375	0.371	0.659
Im $a_{\bar{K}N(I=1)}$	0.606	1.504	0.599	0.605	1.493	0.600

- Cond. (a)  $d_{\bar{K}N, \bar{K}N}$  is fixed to that of the  $I = 0$  case.  
 $d_{\pi\Sigma, \pi\Sigma}$  and  $d_{\bar{K}N, \pi\Lambda}$  are searched to reproduce the complex value of  $a_{\bar{K}N(I=1)}$ .
- Cond. (b)  $d_{\bar{K}N, \bar{K}N}$  and  $d_{\pi\Sigma, \pi\Sigma}$  are fixed to those of the  $I = 0$  case.  
 $d_{\bar{K}N, \pi\Lambda}$  is searched to reproduce the real part of  $a_{\bar{K}N(I=1)}$ .
- Cond. (c) Similar to the condition (b), but  $d_{\bar{K}N, \pi\Lambda}$  is searched to reproduce the imaginary part of  $a_{\bar{K}N(I=1)}$ .

We describe mainly the result obtained with  $f_\pi = 110$  MeV. In the NR case, we can find a set of range parameters which satisfy each condition (a)-(c), as shown in Table 3. However, it is found that in the condition (a) the  $I = 1$  scattering amplitude has a sharp resonance structure slightly below  $\pi\Sigma$  threshold (Fig. 15, left column),<sup>4</sup> although no narrow resonant states in  $I = 1$  sector have been confirmed theoretically and experimentally in such energy region. In the conditions (b) and (c), such a resonance structure does not appear in all the scattering amplitudes (Fig. 15, right column).

In a semi-relativistic case, SR-A, we can find a range parameter set for each condition (a) to (c), in the same way as NRv2. (given in three right columns of Table 3) The scattering amplitudes calculated with the condition

<sup>4</sup>In this case we have found a pole on the complex-energy plane by the ccCSM at  $(E_R, -\Gamma/2) = (1327.2, -1.8)$  MeV. Certainly, this pole exists only by 4 MeV below  $\pi\Sigma$  threshold (=1331 MeV).

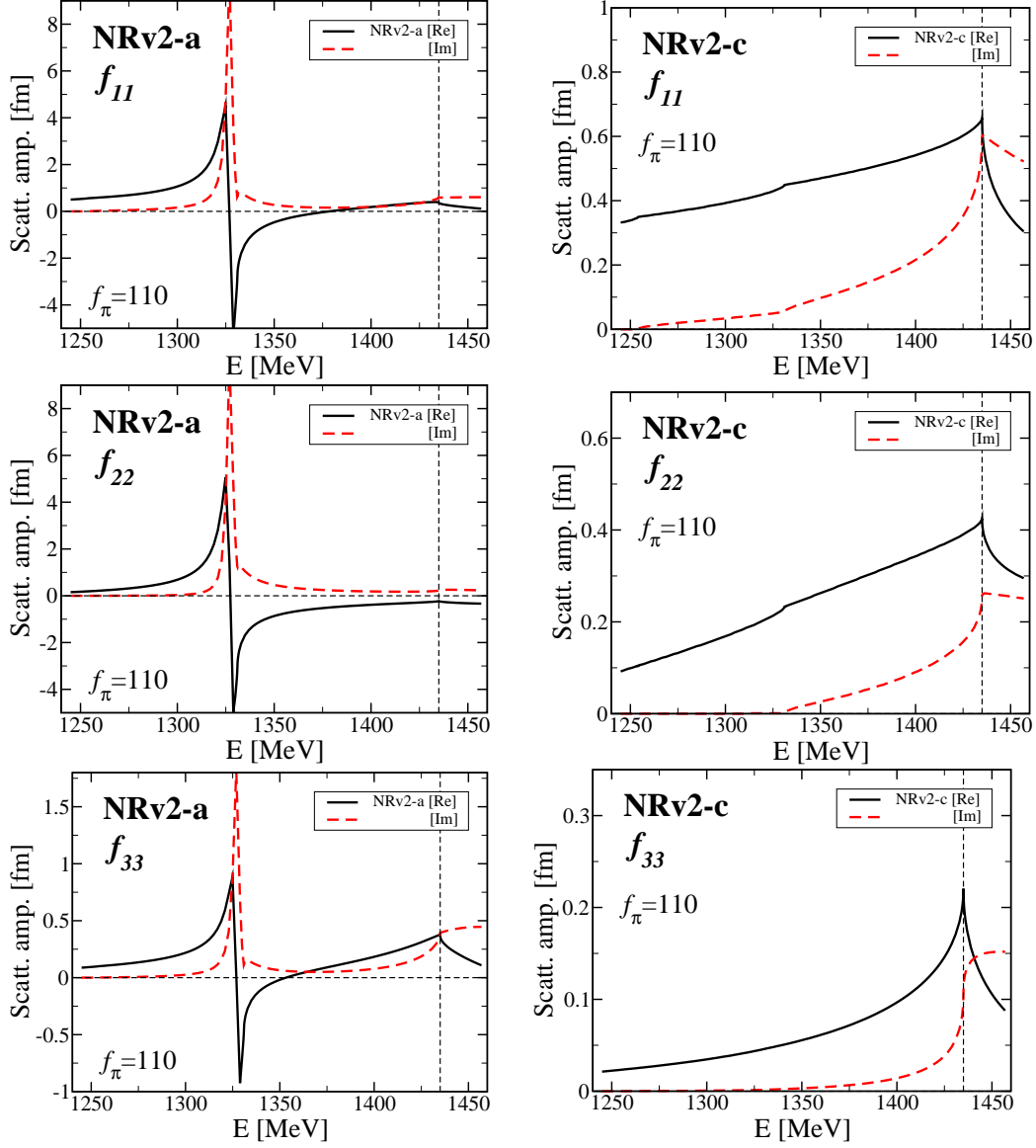


Figure 15:  $I = 1$  scattering amplitudes for NRv2 case with  $f_\pi = 110$  MeV. The real (imaginary) part of scattering amplitude is drawn with a black-solid (red-dashed) line. Left (right) panels are calculated with the condition (a) (condition (c)). Top:  $\bar{K}N \rightarrow \bar{K}N$ , middle:  $\pi\Sigma \rightarrow \pi\Sigma$ , bottom:  $\pi\Lambda \rightarrow \pi\Lambda$ .

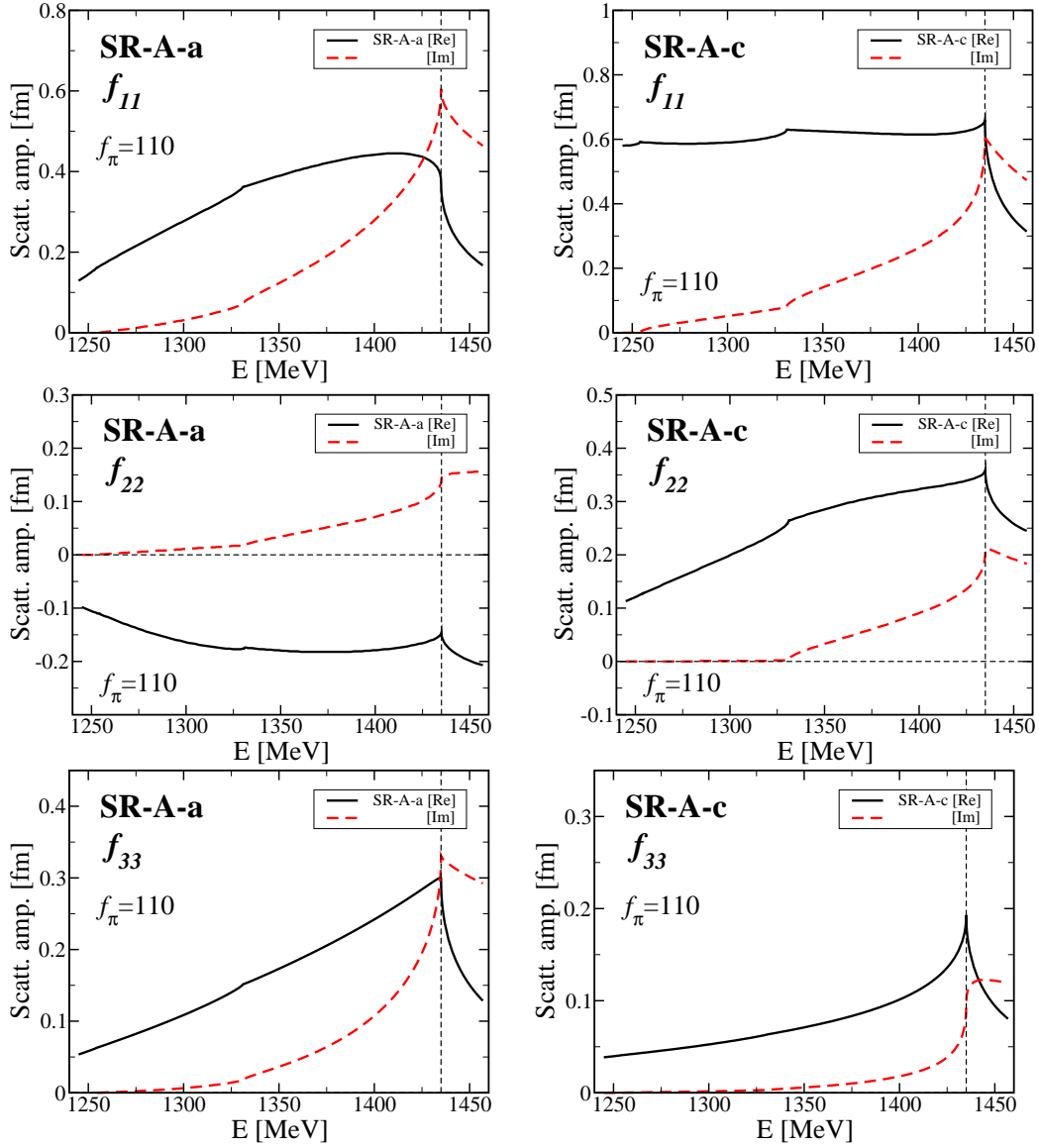


Figure 16:  $I = 1$  scattering amplitudes for SR-A case with  $f_\pi = 110$  MeV. Similar to Fig. 15.

Table 4: Range parameters for the  $I = 1$   $\bar{K}N$ - $\pi\Sigma$ - $\pi\Lambda$  system with the semi-relativistic kinematics (SR-B).  $f_\pi = 110$  MeV. Same as Table 1. Columns “(a)-R1” to “(a)-R3” show the results obtained with the condition (a) relaxed. Details are explained in the text.

Case	SR-B					
Kinematics	Semi-rela.					
Potential	KSW-type					
Condition	(a)	(b)	(c)	(a)-R1	(a)-R2	(a)-R3
$d_{\bar{K}N, \bar{K}N}$	0.369	0.369	0.369	0.369	0.369	0.369
$d_{\pi\Sigma, \pi\Sigma}$	0.248	0.348	0.348	1.800	1.050	0.630
$d_{\bar{K}N, \pi\Lambda}$	0.276	0.157	0.104	0.480	0.530	0.960
Re $a_{\bar{K}N(I=1)}$	0.369	0.075	-0.134	0.858	0.812	0.738
Im $a_{\bar{K}N(I=1)}$	0.600	0.154	0.337	0.600	0.600	0.600

(a) are shown in the left column of Fig. 16. As seen in this figure, the  $\pi\Sigma$  scattering amplitude indicates repulsive nature of  $\pi\Sigma$ - $\pi\Sigma$  channel, in spite that the direct  $\pi\Sigma$  potential is originally attractive. This is considered to be a consequence of the coupled-channel effect. Calculated with the condition (c), all scattering amplitudes of SR-A are quantitatively the same as those of NRv2 with the condition (c) (see the right column of Figs. 15 and 16).

In the other semi-relativistic case, SR-B, a set of range parameters to satisfy the conditions is found only in the condition (a), but is not found in the conditions (b) and (c). The best parameter sets of the conditions (b) and (c) are listed in Table 4. But the scattering  $\bar{K}N$  length calculated with these parameters is far from the Martin’s value. The scattering amplitudes calculated with the condition (a) are shown in the left column of Fig. 17. Compared with those of SR-A (a) in the Fig. 16, they are quantitatively the same as each other. In particular, also in the SR-B (a) the  $\pi\Sigma$  scattering amplitude indicates repulsive nature of  $\pi\Sigma$ - $\pi\Sigma$  channel.

We investigate other  $f_\pi$  values such as 90, 100 and 120 MeV. Range parameters and  $\bar{K}N$  scattering length for these  $f_\pi$ ’s are listed in Table D.7. It is confirmed that the scattering amplitudes for these  $f_\pi$ ’s are essentially the same as those for  $f_\pi = 110$  MeV case above mentioned.

In the remaining part of this section, we consider the cases where the conditions are slightly relaxed. We vary the value of the range parameter  $d_{\bar{K}N, \bar{K}N}$  slightly in the condition (a), since it may be too strict constraint

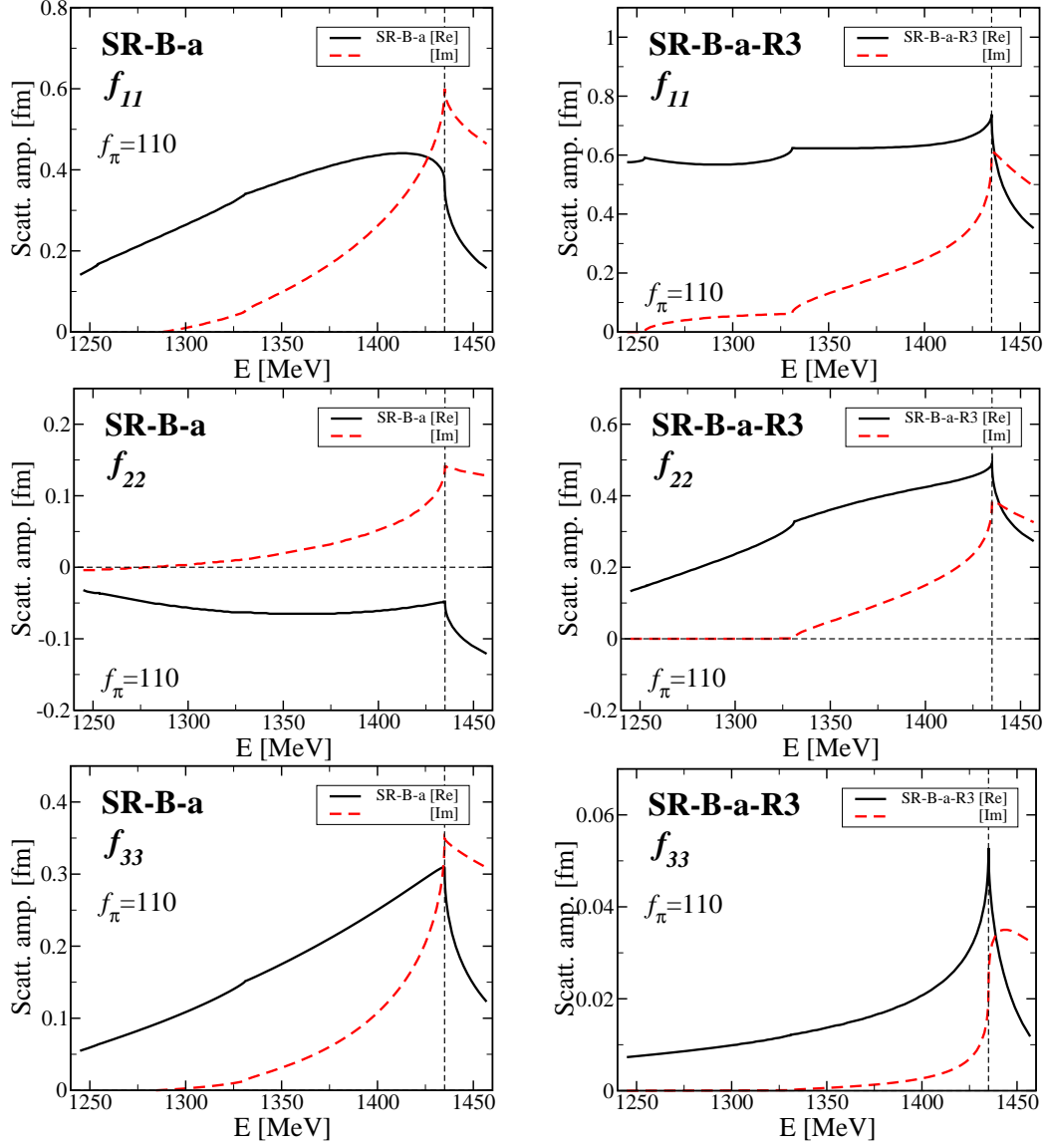


Figure 17:  $I = 1$  scattering amplitudes for SR-B case with  $f_\pi = 110$  MeV. Similar to Fig. 15. Left (right) panels are calculated with the condition (a) (condition (a)-R3).

that  $d_{\bar{K}N, \bar{K}N}$  is fixed to that of the  $I = 0$  sector. With 10% modification of the  $d_{\bar{K}N, \bar{K}N}$ , essential property of the scattering amplitude is found to be unchanged; In both cases of SR-A and SR-B, the  $\pi\Sigma$  scattering amplitude still indicates the repulsive nature, and in the NR a resonance structure is kept to appear around the  $\pi\Sigma$  threshold.

We make an investigation of the SR-B model with a relaxed condition, since this model has a satisfactory range-parameter set only for the condition (a). We relax the condition (a) to give up the simultaneous reproduction of the real and imaginary parts of Martin's value. We examine a single constraint with the imaginary part;  $\text{Im } a_{\bar{K}N(I=1)} = 0.600$  fm. (Call "relaxed condition (a)".) In  $0.1 < d_{\pi\Sigma, \pi\Sigma}, d_{\bar{K}N, \pi\Lambda} < 2.0$ , some sets of  $\{d_{\pi\Sigma, \pi\Sigma}, d_{\bar{K}N, \pi\Lambda}\}$  are obtained under the relaxed condition (a). Typical examples of the parameter sets are listed on the right three columns in Table 4. The parameter sets, (a)-R1, (a)-R2 and (a)-R3, give upper, middle and lower values of  $\text{Re } a_{\bar{K}N(I=1)}$  ranging from 0.738 to 0.858 fm, respectively. The right panels of Fig. 17 show the scattering amplitudes of the SR-B with a parameter set (a)-R3. We note that the  $\pi\Sigma$  scattering amplitude calculated with the relaxed condition (a) indicates attractive nature. The scattering amplitudes of the SR-B (a)-R3 are found to be quite similar to those of NRv2 and SR-A with the condition (c) in all channels, though the magnitude of  $\pi\Lambda$  amplitude is one-order smaller than other cases. (See also right panels of Figs. 15 and 16.) Thus, the scattering amplitudes in  $I = 1$  sector are determined almost independently of the kinematics and potential type, when  $\text{Im } a_{\bar{K}N(I=1)}$  is constrained with the Martin's value.

Note the case that the real part of  $a_{\bar{K}N(I=1)}$  is fixed to the Martin's estimation. We can obtain range-parameter sets with this constraint for SR-B (a). However, it is found that these parameter sets give the imaginary part of  $a_{\bar{K}N(I=1)}$  largely deviated from the Martin's value:  $\text{Im } a_{\bar{K}N(I=1)}$  is obtained to be  $1.2 \sim 1.9$  fm, when  $\text{Re } a_{\bar{K}N(I=1)}$  is fixed to 0.37 fm. Similar results have been obtained also in NRv2 (b) and SR-A (b) as shown in Table 3. We conclude that within our model it is difficult to fix the real part of  $a_{\bar{K}N(I=1)}$  to be the value estimated by Martin, compared to fixing its imaginary part. Thus, we have opted the imaginary part of  $a_{\bar{K}N(I=1)}$  to constrain our model of  $\bar{K}N$ - $\pi Y$  potential in  $I = 1$  channel.

#### 4. Summary and future plan

We have studied a  $\bar{K}N-\pi Y$  system with a coupled-channel complex scaling method (ccCSM) [26] using a chiral SU(3) potential. In our study, scattering states as well as resonant states are investigated within a single framework of ccCSM. Resonance poles are obtained by diagonalizing a complex-scaled Hamiltonian with Gaussian base, similarly to bound states calculation. Scattering problem is solved with an advanced use of ccCSM, “CS-WF” method [28]. In the CS-WF, due to Cauchy’s theorem scattering amplitudes are calculated using complex-scaled wave functions which are also described with Gaussian base. Thus, both of resonance and scattering problems can be solved with Gaussian base and therefore they can be treated with small and straightforward extension of the bound-state calculation. This is the most advantageous point of ccCSM.

Based on Ref. [15] where a meson-baryon potential is derived from a chiral SU(3) theory, we have constructed a meson-baryon potential (KSW-type potential) which is a local potential with Gaussian form in  $r$ -space. Since in the present study it is necessary to deal with pion whose mass is very light, we have examined semi-relativistic kinematics (SR) as well as non-relativistic one (NR). In the NR case, non-relativistically approximated versions of the KSW-type potential are used.

By using the CS-WF method, range parameters of our Gaussian-form potential are determined for both the NR and SR kinematics, so as to reproduce the value of  $\bar{K}N$  scattering length obtained by Martin’s analysis [29]. The scattering amplitudes are investigated with the CS-WF method using the determined potentials. It is interesting that in the SR case we find two sets of the range parameters which give different types of scattering amplitudes. One, denoted as SR-A, is considered to be the relativistic version of the non-relativistic solution, because the scattering amplitudes and the resonance pole have similar properties as those obtained in the NR kinematics. The other one, denoted as SR-B, is unique to the SR kinematics since it shows quite different properties from the NR case.

In the  $I = 0$  sector, a resonance structure is seen below the  $\bar{K}N$  threshold in the  $I = 0$   $\bar{K}N$  and  $\pi\Sigma$  scattering amplitudes. It appears at  $1405 \sim 1420$  MeV in the  $\bar{K}N$  amplitude. It is found that the  $\bar{K}N$  scattering amplitude near the  $\bar{K}N$  threshold is well constrained by the  $\bar{K}N$  scattering length, since its  $f_\pi$  dependence is small and both kinematics give similar results in this region. However, far below the  $\bar{K}N$  threshold the model dependence

of scattering amplitudes becomes prominent; The NR and SR-A cases give qualitatively similar scattering amplitudes, which strongly depends on the  $f_\pi$  value. The SR-B case gives rather different amplitudes from them, especially in the  $\pi\Sigma$  amplitude. We consider that further data far below  $\bar{K}N$  threshold, such as the  $\pi\Sigma$  scattering length, are necessary to reduce such an uncertainty in the deep  $\bar{K}N$  bound region, as pointed out in Ref. [33].

Similarly, the  $I = 1$  sector has also been investigated. When the potential of our model is constrained by the complex value of the  $\bar{K}N$  scattering length with  $I = 1$ , it is found that the scattering amplitude has a resonance structure slightly below the  $\pi\Sigma$  threshold in the NR case, and that  $\pi\Sigma$  scattering amplitude shows repulsive nature in the semi-relativistic cases. However, if the constraint condition for the potential is relaxed so that only the imaginary part of the  $\bar{K}N$  scattering length is reproduced, such a resonance structure disappears in the NR case and the  $\pi\Sigma$  scattering amplitude becomes attractive in the SR cases. We found that it is difficult to constrain our potential model with the real part of the  $\bar{K}N$  scattering length. Under such a constraint condition, the imaginary part is obtained to be largely deviated from the value estimated by Martin.

Compared with other studies, the  $I = 0$  scattering amplitudes obtained in our calculation are a little different. In particular, near the  $\pi\Sigma$  threshold the amplitudes in the present results have larger magnitude than those in Refs. [33] and [19]. One of reasons for this discrepancy is confirmed to be the small difference in the interaction kernel. As another reason, we consider that the Gaussian-form factor in our potential may cause such the enhancement of the scattering amplitudes.

Properties of the resonance pole in the  $I = 0$  sector corresponding to the  $\Lambda(1405)$  have been studied with the usual ccCSM. For  $f_\pi = 90 \sim 120$  MeV, resonance pole is found around

$$(E_R, -\Gamma/2) = \begin{cases} (1418.5 \pm 1.5, -19.5 \pm 5.5) & \text{in NR case,} \\ (1420.5 \pm 3, -24.5 \pm 2) & \text{in SR-A case,} \\ (1419 \pm 1, -13 \pm 2) & \text{in SR-B case,} \end{cases}$$

on the complex-energy plane. The real energy of the pole is well determined to be 1420 MeV, independently of models. The imaginary energy, namely the decay width, depends on the cases. The NR and the SR-A give large value of  $\Gamma/2$ , while it is small in the other semi-relativistic case SR-B. As for the  $f_\pi$  dependence of the pole position, it is found that the NR and the SR-A have similar tendency, but that the SR-B shows different behavior that the

pole energy is quite stable for the change of the  $f_\pi$  value. We have estimated the size of the resonance pole, evaluating a root-mean-square distance with a bi-orthogonal set of complex-scaled wave function. This quantity is not the mean of the physical meson-baryon distance but is expected to give us a guide of it. The obtained meson-baryon mean “distance” is  $1.3 - i0.3$  fm for the NR case and  $1.2 - i0.5$  fm for the two SR cases.

As a result of the present study with the NR and SR kinematics, it is found that  $\bar{K}N$  quantities ( $\bar{K}N$  scattering amplitude, the real energy of  $I = 0$  pole state and its size) near the  $\bar{K}N$  threshold are essentially the same in both the kinematics, when we constrain the model by the  $\bar{K}N$  scattering length that is the quantity at the threshold. However, these two kinematics give largely different results on the quantities far below the  $\bar{K}N$  threshold and those related to  $\pi\Sigma$ , where the relativistic effect becomes important.

In other studies, two poles are reported in  $I = 0$  sector and are related to  $\Lambda(1405)$ . The pole discussed above is considered to be the higher pole of the two poles. As mentioned in the section 3.2, we found a signature of the lower pole around the complex energies of ( $\sim 1360, -90 \sim -40$ ) MeV in a non-relativistic case and ( $1350 \sim 1390, -100 \sim -30$ ) MeV in a semi-relativistic case. However, we can't conclude that this is the lower pole, because its  $\theta$  trajectory is somehow unstable in CSM. We consider that this is due to limitation of numerical accuracy of the CSM with finite number of the Gaussian base for the resonances involving large decay widths. The poles of broad resonances can be investigated by applying an analytic continuation in the coupling constant to the complex scaling method (ACCC+CSM) [40]. It is one of our future plans to carry out ACCC+CSM and clarify whether our potential leads to the double-pole structure or not.

Thus, we have a  $\bar{K}N$ - $\pi Y$  potential for both isospin channels, which is based on a chiral SU(3) theory and is a local Gaussian form in  $r$ -space. In our future plan, we will investigate the three-body system of  $K^-pp$  ( $\bar{K}NN$ - $\pi YN$  system with  $J^\pi = 0^-, T = 1/2$ ) which is the most essential kaonic nuclei. Since the ccCSM can adequately deal with resonant states of a multi-channel system in principle and the CSM is known to be effective for the nuclear many-body study [27], we expect that the ccCSM will give a pole position of the  $K^-pp$  accurately and reveal its structure. We are interested in the role of  $\pi YN$  three-body dynamics, because its implicit/explicit treatment may cause a large difference in the binding of  $K^-pp$  as pointed out in Ref. [41]. It is expected that the contribution of  $\pi YN$  three-body dynamics will be investigated with the ccCSM.

In our analysis, it is worthwhile to use the updated value of the  $\bar{K}N$  scattering length based on the latest data, instead of the Martin's value obtained from old data. The SIDDHARTA group measured quite precisely the shift and width of the  $1s$  atomic level energy of kaonic hydrogen atom [22]. With the  $K^-p$  scattering length based on this data,  $K^-n$  scattering length is estimated with the coupled-channel chiral dynamics [25]. These values of  $K^-p$  and  $K^-n$  scattering lengths are available in our calculation. Furthermore, the SIDDHARTA group is planning to perform experiments on kaonic deuterium in the SIDDHARTA-2 experiment. These forthcoming experiment will constrain more strictly the  $\bar{K}N$  scattering length for both isospin channels [42], though it is pointed out that the analysis with the improved Deser-Trueman relation involves about 10% error on the  $K^-p$  scattering length [43].

Furthermore, the ccCSM approach can be applied to other hadronic systems. For instance, with this method it seems interesting to investigate a few-body system involving  $D$  meson in the charm sector, which is an analogous system with  $\bar{K}$  meson in the strangeness sector [44].

## Acknowledgment

One of authors (A. D.) is thankful to Prof. Kato for his advice on the scattering-amplitude calculation based on the complex scaling method, and to Dr. Hyodo for fruitful discussion on the  $\bar{K}N$  system. He is grateful also to Prof. Oset and Prof. Gal for their useful comments to improve our paper.

## Appendix A. Scattering amplitude for a multi-channel system in non-relativistic kinematics

We consider a Schrödinger equation for a multi-channel system;  $H|\Psi\rangle = E|\Psi\rangle$ . Hamiltonian  $H$  and total wave function  $|\Psi\rangle$  are given as

$$H = \sum_c H_c^0 |c\rangle\langle c| + \sum_{c,c'} V_{cc'} |c\rangle\langle c'|, \quad |\Psi\rangle = \sum_c |\Psi_c\rangle |c\rangle, \quad (\text{A.1})$$

where  $H_c^0$  is the kinetic-energy operator  $\mathbf{p}_c^2/2\mu_c$  for the channel  $c$  and  $V_{cc'}$  is a potential between channels  $c$  and  $c'$ .  $|\Psi_c\rangle$  is a wave function of a channel  $c$ . Projecting the Schrödinger equation onto a channel  $c$ , we get such an equation for the  $c$ -channel wave function as

$$H_c^0 |\Psi_c\rangle + \sum_{c'} V_{cc'} |\Psi_{c'}\rangle = E |\Psi_c\rangle. \quad (\text{A.2})$$

When the incident channel is  $c_0$  and the incoming wave function is given as  $|\phi_{c_0, \mathbf{k}_{c_0}}\rangle$ , the above equation can be modified formally as

$$|\Psi_c^{(c_0)}\rangle = |\phi_{c_0, \mathbf{k}_{c_0}}\rangle \delta_{cc_0} + \frac{1}{E - H_c^0 + i\epsilon} \sum_{c'} V_{cc'} |\Psi_{c'}^{(c_0)}\rangle, \quad (\text{A.3})$$

taking into account the outgoing boundary condition appropriately. Here, we write the incoming channel  $c_0$  on the wave function of each channel explicitly. The above equation is expressed in  $r$ -space as

$$\begin{aligned} \Psi_c^{(c_0)}(\mathbf{r}_c) &= \phi_{c_0, \mathbf{k}_{c_0}}(\mathbf{r}_{c_0}) \delta_{cc_0} \\ &+ \sum_{c'} \int d\mathbf{r}'_c G_c(\mathbf{r}_c, \mathbf{r}'_c; E) \langle \mathbf{r}'_c | V_{cc'} | \Psi_{c'}^{(c_0)} \rangle, \end{aligned} \quad (\text{A.4})$$

where  $G_c(\mathbf{r}_c, \mathbf{r}'_c; E)$  is a Green function in the channel  $c$ . By performing complex integral as shown in many textbooks, it becomes

$$G_c(\mathbf{r}_c, \mathbf{r}'_c; E) = \langle \mathbf{r}_c | \frac{1}{E - H_c^0 + i\epsilon} | \mathbf{r}'_c \rangle = -\frac{1}{4\pi} \frac{2\mu_c}{\hbar^2} \frac{e^{ik_c|\mathbf{r}_c - \mathbf{r}'_c|}}{|\mathbf{r}_c - \mathbf{r}'_c|} \quad (\text{A.5})$$

$$\simeq -\frac{1}{4\pi} \frac{2\mu_c}{\hbar^2} \frac{e^{ik_c r_c}}{r_c} e^{-i\mathbf{k}_c \cdot \mathbf{r}'_c} \quad (|\mathbf{r}_c| \gg |\mathbf{r}'_c|), \quad (\text{A.6})$$

where  $\mathbf{k}_c = k_c \mathbf{r}_c / r_c$  and  $r_c = |\mathbf{r}_c|$ . Then, the channel- $c$  wave function becomes

$$\Psi_c^{(c_0)}(\mathbf{r}_c) = \phi_{c_0}(\mathbf{r}_{c_0}) \delta_{cc_0} + \frac{e^{ik_c r_c}}{r_c} \times \left( -\frac{1}{4\pi} \right) \frac{2\mu_c}{\hbar^2} \sum_{c'} \langle \phi_{c, \mathbf{k}_c} | V_{cc'} | \Psi_{c'}^{(c_0)} \rangle, \quad (\text{A.7})$$

using the fact that the function  $\phi_{c, \mathbf{k}_c}(\mathbf{r}_c)$  is  $e^{i\mathbf{k}_c \cdot \mathbf{r}_c}$ . Substituting the channel- $c$  wave function in Eq. (A.1) with the above expression, the total wave function is given as

$$|\Psi\rangle = \phi_{c_0}(\mathbf{r}_{c_0}) |c_0\rangle + \sum_c \frac{e^{ik_c r_c}}{r_c} |c\rangle \cdot \left( -\frac{1}{4\pi} \right) \frac{2\mu_c}{\hbar^2} \sum_{c'} \langle \phi_{c, \mathbf{k}_c} | V_{cc'} | \Psi_{c'}^{(c_0)} \rangle. \quad (\text{A.8})$$

Therefore, the scattering amplitude between the initial channel  $c_0$  and the final channel  $c$  is

$$f_{cc_0}(\mathbf{k}_c, \mathbf{k}_{c_0}) = -\frac{1}{4\pi} \frac{2\mu_c}{\hbar^2} \sum_{c'} \langle \phi_{c, \mathbf{k}_c} | V_{cc'} | \Psi_{c'}^{(c_0)} \rangle. \quad (\text{A.9})$$

The wave functions  $\phi_{c,\mathbf{k}_c}(\mathbf{r}) = e^{i\mathbf{k}_c \cdot \mathbf{r}}$  and  $\Psi_{c'}^{(c_0)}(\mathbf{r})$  are expanded on partial waves  $l$  as

$$\phi_{c,\mathbf{k}_c}(\mathbf{r}) = 4\pi \sum_{l,m} i^l \frac{\hat{j}_l(k_c r)}{k_c r} Y_{lm}^*(\Omega_{\mathbf{k}_c}) Y_{lm}(\Omega_{\mathbf{r}}), \quad (\text{A.10})$$

$$\Psi_c^{(c_0)}(\mathbf{r}) = 4\pi \sum_{l,m} i^l \frac{\psi_{l,c}^{(c_0)}(r)}{k_{c_0} r} Y_{lm}^*(\Omega_{\mathbf{k}_{c_0}}) Y_{lm}(\Omega_{\mathbf{r}}) \quad (\text{A.11})$$

and the scattering amplitude is expanded on the orbital angular momentum as

$$f_{cc_0}(\mathbf{k}_c, \mathbf{k}_{c_0}) = \sum_l (2l+1) P_l(\cos \theta_{(\mathbf{k}_c, \mathbf{k}_{c_0})}) f_{l,cc_0}(k_c, k_{c_0}). \quad (\text{A.12})$$

Thus, expanding Eq. (A.9) for the partial waves using Eqs. (A.10)-(A.12), the scattering amplitude for the partial wave  $l$  is given as

$$f_{l,cc_0}(k_c, k_{c_0}) = -\frac{2\mu_c}{\hbar^2 k_c k_{c_0}} \sum_{c'} \langle \hat{j}_l(k_c r) | V_{cc'} | \psi_{l,c'}^{(c_0)}(r) \rangle, \quad (\text{A.13})$$

if the potential  $V_{cc'}$  is a central potential.

## Appendix B. Scattering amplitude in semi-relativistic kinematics

We give the formula of the scattering amplitude for a semi-relativistic Hamiltonian. We derive it by using Green function in the same way as the non-relativistic case explained in Appendix A. In the semi-relativistic case, the kinetic term of Hamiltonian is

$$H_c^0 = \sqrt{m_c^2 + \hat{\mathbf{p}}_c^2} + \sqrt{M_c^2 + \hat{\mathbf{p}}_c^2}. \quad (\text{B.1})$$

We consider the Green function for this  $H_c^0$ :

$$\left\{ E - \left( \sqrt{m^2 + \hat{\mathbf{p}}^2} + \sqrt{M^2 + \hat{\mathbf{p}}^2} \right) \right\} G^{(+)}(\mathbf{r}, \mathbf{r}'; E) = \delta^3(\mathbf{r} - \mathbf{r}'). \quad (\text{B.2})$$

Hereafter, we drop the channel suffix ‘‘ $c$ ’’ because the following calculation is considered just in the channel  $c$ .

By the Fourier transformation,  $G^{(+)}(\mathbf{r}, \mathbf{r}')$  and  $\delta^3(\mathbf{r} - \mathbf{r}')$  are expressed as

$$G^{(+)}(\mathbf{r}, \mathbf{r}') = (2\pi)^{-3} \int d\mathbf{k} \tilde{G}(\mathbf{k}) e^{i\mathbf{k}\cdot(\mathbf{r}-\mathbf{r}')}, \quad (\text{B.3})$$

$$\delta^3(\mathbf{r} - \mathbf{r}') = (2\pi)^{-3} \int d\mathbf{k} e^{i\mathbf{k}\cdot(\mathbf{r}-\mathbf{r}')}. \quad (\text{B.4})$$

Using these equations, Eq. (B.2) becomes

$$\left\{ E - \left( \sqrt{m^2 + \hbar^2 \mathbf{k}^2} + \sqrt{M^2 + \hbar^2 \mathbf{k}^2} \right) \right\} \tilde{G}(\mathbf{k}) = 1. \quad (\text{B.5})$$

Then, the Green function in the momentum space,  $\tilde{G}(\mathbf{k})$ , is

$$\tilde{G}(\mathbf{k}) = \{E - (\omega(\mathbf{k}) + \Omega(\mathbf{k}))\}^{-1}, \quad (\text{B.6})$$

$$\omega(\mathbf{k}) = \sqrt{m^2 + \hbar^2 \mathbf{k}^2}, \quad \Omega(\mathbf{k}) = \sqrt{M^2 + \hbar^2 \mathbf{k}^2}. \quad (\text{B.7})$$

Inserting this equation into Eq. (B.3) and integrating on angular directions, we obtain

$$G^{(+)}(\mathbf{r}, \mathbf{r}') = (2\pi)^{-2} (i|\mathbf{r} - \mathbf{r}'|)^{-1} \times \int_{-\infty}^{\infty} k dk \{E - (\omega(k) + \Omega(k))\}^{-1} e^{ik|\mathbf{r}-\mathbf{r}'|}. \quad (\text{B.8})$$

We rationalize  $\{E - (\omega(k) + \Omega(k))\}^{-1}$  in terms of  $\hbar^2 k^2$ . After tiresome algebraic calculation, we obtain

$$\frac{1}{E - (\omega(k) + \Omega(k))} = \frac{(\text{Num.})}{(\text{Den.})}, \quad (\text{B.9})$$

$$(\text{Num.}) = \{E + (\omega + \Omega)\} \{E - (\omega - \Omega)\} \{E + (\omega - \Omega)\}, \quad (\text{B.10})$$

$$(\text{Den.}) = -4E^2 \hbar^2 \left[ k^2 - \frac{E^2 - (m - M)^2}{2E\hbar} \frac{E^2 - (m + M)^2}{2E\hbar} \right]. \quad (\text{B.11})$$

When we define a variable  $k_0$  as

$$k_0 \equiv \sqrt{\frac{E^2 - (m - M)^2}{2E\hbar} \frac{E^2 - (m + M)^2}{2E\hbar}}, \quad (\text{B.12})$$

then

$$\frac{1}{E - (\omega(k) + \Omega(k))} = \frac{(\text{Num.})}{-4E^2 \hbar^2} \left( \frac{1}{k - k_0} + \frac{1}{k + k_0} \right) \frac{1}{2k}. \quad (\text{B.13})$$

Inserting this into Eq. (B.8),

$$G^{(+)}(\mathbf{r}, \mathbf{r}') = (2\pi)^{-2} (i|\mathbf{r} - \mathbf{r}'|)^{-1} (-8E^2\hbar^2)^{-1} \\ \times \int_{-\infty}^{\infty} dk (Num.) \left( \frac{1}{k - (k_0 + i\epsilon)} + \frac{1}{k + (k_0 + i\epsilon)} \right) \\ \times e^{ik|\mathbf{r} - \mathbf{r}'|}. \quad (\text{B.14})$$

Here, we add  $i\epsilon$  to  $k_0$  in order to satisfy the outgoing boundary condition in the later calculation. By the principal integration, we pick up the pole  $k = k_0 + i\epsilon$ . At the limit of  $\epsilon \rightarrow 0$ , then the Green function is

$$G^{(+)}(\mathbf{r}, \mathbf{r}') = \frac{e^{ik_0|\mathbf{r} - \mathbf{r}'|}}{|\mathbf{r} - \mathbf{r}'|} \times (-16\pi E^2\hbar^2)^{-1} (Num.)_{k=k_0} \quad (\text{B.15})$$

Finally, we consider the last term  $(Num.)_{k=k_0}$ . After bothersome calculation using the definition of  $k_0$  (Eq. (B.12)), we obtain

$$\omega(k_0) = \frac{E^2 + m^2 - M^2}{2E}, \quad \Omega(k_0) = \frac{E^2 - m^2 + M^2}{2E}. \quad (\text{B.16})$$

Here we notice that  $\omega(k_0) + \Omega(k_0) = E$ . This is a trivial equation because it indicates energy conservation. Using this fact, we can simplify the term  $(Num.)_{k=k_0}$  to be

$$(Num.)_{k=k_0} = \{E + (\omega + \Omega)\}_{k=k_0} \{E - (\omega - \Omega)\}_{k=k_0} \{E + (\omega - \Omega)\}_{k=k_0} \\ = 8E \omega(k_0) \Omega(k_0) \quad (\text{B.17})$$

Inserting this result into Eq. (B.15), then

$$G^{(+)}(\mathbf{r}, \mathbf{r}') = \frac{e^{ik_0|\mathbf{r} - \mathbf{r}'|}}{|\mathbf{r} - \mathbf{r}'|} \times \left( -\frac{1}{2\pi} \right) \frac{1}{\hbar^2} \frac{\omega(k_0) \Omega(k_0)}{E}. \quad (\text{B.18})$$

By remembering  $\omega(k = k_0) + \Omega(k = k_0) = E$  and the definition of the reduced energy as  $\tilde{\omega} \equiv \omega\Omega/(\omega + \Omega)$ , we obtain the Green function for the channel  $c$  in the semi-relativistic kinematics:

$$G_c^{(+)}(\mathbf{r}_c, \mathbf{r}'_c) = -\frac{1}{4\pi} \frac{2\tilde{\omega}_c(k_c)}{\hbar^2} \frac{e^{ik_c|\mathbf{r}_c - \mathbf{r}'_c|}}{|\mathbf{r}_c - \mathbf{r}'_c|}, \quad (\text{B.19})$$

where the suffix of channel  $c$  is recovered and  $k_c$  is  $k_0$  given as Eq. (B.12) in the channel  $c$ . Compared with the non-relativistic case (Eq. (A.5)), it is

found that the reduced mass  $\mu_c$  is simply replaced with the reduced energy  $\tilde{\omega}_c$ . Since the remaining part of calculation is completely the same as that for the non-relativistic case, the scattering amplitude for the semi-relativistic kinematics is obtained to be

$$f_{l,cc_0}(k_c, k_{c_0}) = -\frac{2\tilde{\omega}_c}{\hbar^2 k_c k_{c_0}} \sum_{c'} \langle \hat{j}_l(k_c r) | V_{cc'} | \psi_{l,c'}^{(c_0)}(r) \rangle, \quad (\text{B.20})$$

by replacing  $\mu_c$  in Eq. (A.9) with  $\tilde{\omega}_c$ .

### Appendix C. Matrix element of the kinetic term in the semi-relativistic case

In the semi-relativistic kinematics, the kinetic energy and mass terms in the Hamiltonian are of the form of  $\sqrt{m^2 + \hat{\mathbf{p}}^2} + \sqrt{M^2 + \hat{\mathbf{p}}^2}$  as shown in Eq. (2). In this article, a wave function is expanded in terms of partial waves;  $\Psi(\mathbf{r}) = \sum_{lm} r^{-1} \psi_l(r) Y_{lm}(\Omega)$ . Furthermore its radial part is expanded with a Gaussian base, as Eq.(14) and Eq.(24) explained in non-relativistic case;

$$\psi_l(r)/r = \sum_j C_j^l G_j^l(r)/r, \quad G_j^l(r) = N_l(b_j) r^{l+1} \exp[-r^2/2b_j^2], \quad (\text{C.1})$$

where  $N_l(b_j)$  means a normalization factor. We need to calculate the matrix element  $\langle r^{-1} G_i^l Y_{lm} | \sqrt{m^2 + \hat{\mathbf{p}}^2} | r^{-1} G_j^{l'} Y_{l'm'} \rangle$ . This matrix element is calculated as follows:

$$\begin{aligned} & \langle \frac{1}{r} G_i^l Y_{lm} | \sqrt{m^2 + \hat{\mathbf{p}}^2} | \frac{1}{r} G_j^{l'} Y_{l'm'} \rangle \\ &= \int dr dr' d\mathbf{q} d\mathbf{q}' \langle \frac{1}{r} G_i^l Y_{lm} | \mathbf{r} \rangle \langle \mathbf{r} | \mathbf{q} \rangle \langle \mathbf{q} | \sqrt{m^2 + \hat{\mathbf{p}}^2} | \mathbf{q}' \rangle \langle \mathbf{q}' | \mathbf{r}' \rangle \langle \mathbf{r}' | \frac{1}{r} G_j^{l'} Y_{l'm'} \rangle \\ &= \delta_{ll'} \delta_{mm'} \frac{2}{\pi} \int_0^\infty dq q^2 \sqrt{m^2 + q^2} \\ & \quad \times \int_0^\infty dr G_i^l(r) j_l(qr) \times \int_0^\infty dr' G_j^{l'}(r') j_l(qr'), \end{aligned} \quad (\text{C.2})$$

where  $\langle \mathbf{r} | \mathbf{q} \rangle = e^{i\mathbf{q}\cdot\mathbf{r}}$  and its expansion (Eq. (A.10)) is used. In case of  $s$ -wave ( $l = 0$ ) which we are considering in this article, the last integration for  $r$  and  $r'$  variables can be performed analytically. Finally, the above matrix element

for a complex-scaled  $\hat{\mathbf{p}}$  is expressed as

$$\begin{aligned} & \langle \frac{1}{r} G_i^0 Y_{00} | \sqrt{m^2 + (\hat{\mathbf{p}} e^{-i\theta})^2} | \frac{1}{r} G_j^0 Y_{00} \rangle \\ &= \frac{4}{\sqrt{\pi}} (b_i b_j)^{3/2} \int_0^\infty dq q^2 \sqrt{m^2 + q^2 e^{-2i\theta}} \exp \left[ -\frac{1}{2} (b_i^2 + b_j^2) q^2 \right]. \end{aligned} \quad (\text{C.3})$$

The integration for the variable  $q$  is carried out numerically. The matrix element of Eq. (C.3) is used when we diagonalize the complex-scaled Hamiltonian to find resonance poles as explained in section 2.2 and we calculate a complex-scaled wave function as shown in Eq. (25) to obtain scattering amplitudes.

Note that in a semi-relativistic case any wave number  $k$  is calculated from  $\sqrt{m^2 + \hbar k^2} + \sqrt{M^2 + \hbar k^2} = E$  and that any reduced mass  $\mu$  in a non-relativistic case is replaced with corresponding reduced energy  $\omega = E_M E_B / (E_M + E_B)$  where  $E_M$  and  $E_B$  mean meson and baryon energies, respectively;  $E_M = \sqrt{m^2 + \hbar k^2}$  and  $E_B = \sqrt{M^2 + \hbar k^2}$ .

#### Appendix D. Detailed results of $f_\pi = 90, 100, 120$ MeV cases

We show the results for the cases of  $f_\pi = 90, 100$  and  $120$  MeV. Tables D.5, D.6, D.7 and D.8 correspond to Tables 1, 2, 3 and 4 which are for the case of  $f_\pi = 110$  MeV, respectively.

#### References

- [1] Y. Akaishi and T. Yamazaki, Phys. Rev. C **65**, 044005 (2002); T. Yamazaki and Y. Akaishi, Phys. Lett. B **535**, 70 (2002).
- [2] A. Doté, H. Horiuchi, Y. Akaishi and T. Yamazaki, Phys. Lett. B **590**, 51 (2004); Phys. Rev. C **70**, 044313 (2004).
- [3] D. Gazda, E. Friedman, A. Gal and J. Mares, Phys. Rev. C **76**, 055204 (2007); Phys. Rev. C **77**, 045206 (2008). A. Cieply, E. Friedman, A. Gal, D. Gazda and J. Mares, Phys. Rev. C **84**, 045206 (2011).
- [4] T. Muto, T. Maruyama and T. Tatsumi, Phys. Rev. C **79**, 035207 (2009).
- [5] Y. Ikeda and T. Sato, Phys. Rev. C **76**, 035203 (2007).

Table D.5: Range parameters for  $I = 0$   $\bar{K}N$ - $\pi\Sigma$  system. All quantities are in unit of fm.  $f_\pi = 90, 100$  and  $120$  MeV cases. Corresponding to Table 1.

Case	NRv1	NRv2	SR-A	SR-B
Kinematics	Non-rela.		Semi-rela.	
Potential	NRv1	NRv2	KSW-type	
$f_\pi = 90$				
$d_{\bar{K}N, \bar{K}N}$	0.576	0.574	0.635	0.487
$d_{\pi\Sigma, \pi\Sigma}$	0.725	0.751	0.830	0.457
Re $a_{\bar{K}N(I=0)}$	-1.700	-1.700	-1.702	-1.703
Im $a_{\bar{K}N(I=0)}$	0.677	0.687	0.685	0.677
$f_\pi = 100$				
$d_{\bar{K}N, \bar{K}N}$	0.503	0.501	0.561	0.421
$d_{\pi\Sigma, \pi\Sigma}$	0.665	0.695	0.770	0.395
Re $a_{\bar{K}N(I=0)}$	-1.702	-1.702	-1.698	-1.703
Im $a_{\bar{K}N(I=0)}$	0.680	0.683	0.679	0.673
$f_\pi = 120$				
$d_{\bar{K}N, \bar{K}N}$	0.386	0.384	0.446	0.327
$d_{\pi\Sigma, \pi\Sigma}$	0.549	0.581	0.659	0.310
Re $a_{\bar{K}N(I=0)}$	-1.699	-1.700	-1.697	-1.690
Im $a_{\bar{K}N(I=0)}$	0.674	0.669	0.672	0.669

- [6] N. V. Shevchenko, A. Gal and J. Mares, Phys. Rev. Lett. **98**, 082301 (2007). N. V. Shevchenko, A. Gal, J. Mares and J. Révai, Phys. Rev. C **76**, 044004 (2007).
- [7] A. Doté, T. Hyodo and W. Weise, Nucl. Phys. A **804**, 197 (2008); Phys. Rev. C **79**, 014003 (2009).
- [8] S. Wycech and A. M. Green, Phys. Rev. C **79**, 014001 (2009).
- [9] N. Barnea, A. Gal and E. Z. Liverts, Phys. Lett. B **712**, 132 (2012).
- [10] A. Gal, Prog. Theor. Phys. Suppl. **186**, 270 (2010).
- [11] M. Agnello *et al.* (FINUDA collaboration), Phys. Rev. Lett. **94**, 212303 (2005).
- [12] T. Yamazaki *et al.* (DISTO collaboration), Phys. Rev. Lett. **104**, 132502 (2010).

Table D.6: Pole position of the  $I = 0$   $\bar{K}N$ - $\pi\Sigma$  system and the meson-baryon distance in the pole state.  $f_\pi = 90, 100$  and  $120$  MeV cases. Corresponding to Table 2.

Case	NRv1	NRv2	SR-A	SR-B
Kinematics	Non-rela.		Semi-rela.	
Potential	NRv1	NRv2	KSW-type	
$f_\pi = 90$				
$E_R$	1419.8	1419.9	1423.6	1419.0
$\Gamma/2$	26.0	23.1	26.4	14.4
$(B_{\bar{K}N})$	(15.2)	(15.1)	(11.4)	(16.0)
$\sqrt{\langle r^2 \rangle}_{\bar{K}N+\pi\Sigma}$	$1.20 - 0.28i$	$1.25 - 0.29i$	$1.20 - 0.42i$	$1.21 - 0.49i$
$f_\pi = 100$				
$E_R$	1417.3	1418.0	1421.5	1419.6
$\Gamma/2$	23.1	19.8	26.3	13.2
$(B_{\bar{K}N})$	(17.7)	(17.0)	(13.5)	(15.4)
$\sqrt{\langle r^2 \rangle}_{\bar{K}N+\pi\Sigma}$	$1.31 - 0.29i$	$1.36 - 0.30i$	$1.22 - 0.43i$	$1.21 - 0.49i$
$f_\pi = 120$				
$E_R$	1416.9	1418.3	1417.5	1418.9
$\Gamma/2$	16.7	14.0	22.9	11.7
$(B_{\bar{K}N})$	(18.1)	(16.7)	(17.5)	(16.1)
$\sqrt{\langle r^2 \rangle}_{\bar{K}N+\pi\Sigma}$	$1.38 - 0.38i$	$1.44 - 0.38i$	$1.20 - 0.49i$	$1.16 - 0.42i$

- [13] V. K. Magas, E. Oset, A. Ramos and H. Toki, Phys. Rev. C **74**, 025206 (2006).
- [14] N. Isgur and G. Karl, Phys. Rev. D **18**, 4187 (1978).
- [15] N. Kaiser, P. B. Siegel and W. Weise, Nucl. Phys. A **594**, 325 (1995).
- [16] E. Oset and A. Ramos, Nucl. Phys. A **635**, 99 (1998).
- [17] Summarized in T. Hyodo and D. Jido, Prog. Part. Nucl. Phys. **67**, 55 (2012).
- [18] D. Jido, J. A. Oller, E. Oset, A. Ramos and U. -G. Meißner, Nucl. Phys. A **725**, 181 (2003).
- [19] T. Hyodo and W. Weise, Phys. Rev. C **77**, 035204 (2008).

Table D.7: Range parameters for  $I = 1$   $\bar{K}N$ - $\pi\Sigma$ - $\pi\Lambda$  system with non-relativistic kinematics (NRv2, left three columns) and semi-relativistic kinematics (SR-A, right three columns).  $f_\pi = 90, 100, 120$  MeV cases. Corresponding to Tables 3.

Case	NRv2			SR-A		
Kinematics	Non-rela.			Semi-rela.		
Potential	NRv2			KSW-type		
Condition	(a)	(b)	(c)	(a)	(b)	(c)
$f_\pi = 90$						
$d_{\bar{K}N, \bar{K}N}$	0.574	0.574	0.574	0.635	0.635	0.635
$d_{\pi\Sigma, \pi\Sigma}$	0.221	0.751	0.751	0.334	0.830	0.830
$d_{\bar{K}N, \pi\Lambda}$	0.391	0.558	1.138	0.413	0.556	0.942
Re $a_{\bar{K}N(I=1)}$	0.371	0.370	0.621	0.365	0.368	0.624
Im $a_{\bar{K}N(I=1)}$	0.601	1.358	0.600	0.600	1.353	0.600
$f_\pi = 100$						
$d_{\bar{K}N, \bar{K}N}$	0.501	0.501	0.501	0.561	0.561	0.561
$d_{\pi\Sigma, \pi\Sigma}$	0.186	0.695	0.695	0.293	0.770	0.770
$d_{\bar{K}N, \pi\Lambda}$	0.289	0.394	0.663	0.336	0.431	0.631
Re $a_{\bar{K}N(I=1)}$	0.367	0.368	0.626	0.372	0.366	0.629
Im $a_{\bar{K}N(I=1)}$	0.601	1.452	0.600	0.598	1.438	0.600
$f_\pi = 120$						
$d_{\bar{K}N, \bar{K}N}$	0.384	0.384	0.384	0.446	0.446	0.446
$d_{\pi\Sigma, \pi\Sigma}$	0.139	0.581	0.581	0.236	0.659	0.659
$d_{\bar{K}N, \pi\Lambda}$	0.173	0.240	0.324	0.242	0.301	0.370
Re $a_{\bar{K}N(I=1)}$	0.382	0.369	0.689	0.359	0.365	0.691
Im $a_{\bar{K}N(I=1)}$	0.608	1.539	0.601	0.603	1.542	0.600

- [20] V. K. Magas, E. Oset and A. Ramos, Phys. Rev. Lett. **95**, 052301 (2005).  
D. Jido, E. Oset and T. Sekihara, Eur. Phys. J. A **42**, 257 (2009).  
T. Hyodo, A. Hosaka, E. Oset, A. Ramos and M. J. Vicente Vacas, Phys. Rev. C **68**, 065203 (2003).
- [21] N. V. Shevchenko, Phys. Rev. C **85**, 034001 (2012).
- [22] M. Bazzi *et al.* (SIDDHARTA collaboration), Phys. Lett. B **704**, 113 (2011); Nucl. Phys. A **881**, 88 (2012).
- [23] D. W. Thomas, A. Engler, H. E. Fisk and R. W. Kraemer, Nucl. Phys. B **56**, 15 (1973). R. J. Hemingway, Nucl. Phys. B **253**, 742 (1985). S.

Table D.8: Range parameters for the  $I = 1$   $\bar{K}N$ - $\pi\Sigma$ - $\pi\Lambda$  system with the semi-relativistic kinematics (SR-B).  $f_\pi = 90, 100, 120$  MeV cases. Corresponding to Table 4.

Case	SR-B					
Kinematics	Semi-rela.					
Potential	KSW-type					
Condition	(a)	(b)	(c)	(a)-R1	(a)-R2	(a)-R3
$f_\pi = 90$						
$d_{\bar{K}N, \bar{K}N}$	0.487	0.487	0.487	0.487	0.487	0.487
$d_{\pi\Sigma, \pi\Sigma}$	0.313	0.457	0.457	0.930	0.960	1.340
$d_{\bar{K}N, \pi\Lambda}$	0.422	0.187	0.100	1.880	1.510	0.930
Re $a_{\bar{K}N(I=1)}$	0.374	0.072	-0.145	0.966	0.928	0.869
Im $a_{\bar{K}N(I=1)}$	0.602	0.268	0.404	0.600	0.600	0.600
$f_\pi = 100$						
$d_{\bar{K}N, \bar{K}N}$	0.421	0.421	0.421	0.421	0.421	0.421
$d_{\pi\Sigma, \pi\Sigma}$	0.277	0.395	0.395	1.870	0.740	0.850
$d_{\bar{K}N, \pi\Lambda}$	0.335	0.174	0.100	0.610	1.440	0.910
Re $a_{\bar{K}N(I=1)}$	0.366	0.057	-0.153	0.855	0.825	0.793
Im $a_{\bar{K}N(I=1)}$	0.601	0.189	0.351	0.599	0.600	0.599
$f_\pi = 120$						
$d_{\bar{K}N, \bar{K}N}$	0.327	0.327	0.327	0.327	0.327	0.327
$d_{\pi\Sigma, \pi\Sigma}$	0.223	0.310	0.310	1.400	0.810	0.520
$d_{\bar{K}N, \pi\Lambda}$	0.236	0.140	0.105	0.400	0.450	0.910
Re $a_{\bar{K}N(I=1)}$	0.379	0.123	-0.097	0.859	0.799	0.698
Im $a_{\bar{K}N(I=1)}$	0.600	0.141	0.360	0.601	0.600	0.599

- Prakhov *et al.* (Crystal Ball collaboration), Phys. Rev. C **70**, 034605 (2004). I. Zychor *et al.*, Phys. Lett. B **660**, 167 (2008).
- [24] D. N. Tovee *et al.*, Nucl. Phys. B **33**, 493 (1971). R. J. Nowak *et al.*, Nucl. Phys. B **139**, 61 (1978).
- [25] Y. Ikeda, T. Hyodo and W. Weise, Phys. Lett. B **706**, 63 (2011); Nucl. Phys. A **881**, 98 (2012).
- [26] S. Aoyama, T. Myo, K. Kato, and K. Ikeda, Prog. Theor. Phys. **116**, 1 (2006).
- [27] T. Myo, R. Ando and K. Kato, Phys. Lett. B **691**, 150 (2010).
- [28] A. T. Kruppa, R. Suzuki and K. Kato, Phys. Rev. C **75**, 044602 (2007).
- [29] A. D. Martin, Nucl. Phys. B **179**, 33 (1981).
- [30] G. Garcia-Calderon and R. Peierls, Nucl. Phys. A **265**, 443 (1976).
- [31] A. Doté, T. Inoue and T. Myo, Proceedings of “International conference on the structure of baryons (BARYONS’10) ”, AIP Conference Proceedings Volume 1388, page 589. (ISBN: 978-0-7354-0952-1)
- [32] R. Suzuki, A. T. Kruppa, B. G. Giraud and K. Kato, Prog. Theor. Phys. **119**, 949 (2008).
- [33] Y. Ikeda, T. Hyodo, D. Jido, H. Kamano, T. Sato and K. Yazaki, Prog. Theor. Phys. **125**, 1205 (2011).
- [34] J. Yamagata-Sekihara, J. Nieves and E. Oset, Phys. Rev. D **83**, 014003 (2011).
- [35] T. Sekihara, T. Hyodo and D. Jido, Phys. Rev. C **83**, 055202 (2011).
- [36] S. Takeuchi and K. Shimizu, Phys. Rev. C **79**, 045204 (2009).
- [37] M. Homma, T. Myo and K. Kato, Prog. Theor. Phys. **97**, 561 (1997) and references therein.
- [38] This is based on the original discussion between Dr. Hyodo and Prof. Yazaki.

- [39] Private communication with Dr. Hyodo.
- [40] S. Aoyama, Phys. Rev. C **68**, 034313 (2003).
- [41] Y. Ikeda and T. Sato, Phys. Rev. C **79**, 035201 (2009).
- [42] SIDDHARTA-2 collaboration. Ref. [40] in the reference [22].
- [43] A. Cieply and J. Smejkal, Eur. Phys. J. A **34**, 237 (2007).
- [44] M. Bayar, C. W. Xiao, T. Hyodo, A. Doté, M. Oka and E. Oset, Phys. Rev. C **86**, 044004 (2012).